UNIVERSITÀ
DEGLI STUDI
DI TRIESTE

UNIVERSITÀ DEGLI STUDI DI TRIESTE

XXXIV CICLO DEL DOTTORATO DI RICERCA IN BIOMEDICINA MOLECOLARE

---

p53 context dependent role of Mir-9/KLF5/Sp1 axis in modulating response to therapy in Head and Neck Squamous Cell Carcinoma

Settore scientifico-disciplinare: **BIO/11 BIOLOGIA MOLECOLARE**

DOTTORANDA
LORENA MUSCO

COORDINATORE
PROF. GERMANA MERONI

SUPERVISORE DI TESI
PROF. GUSTAVO BALDASSARRE

ANNO ACCADEMICO 2020/2021

A come tutto è iniziato;

A tutto ciò che è cambiato.

The main part of the results included in this PhD thesis has been published on “mir-9 modulates and predicts the response to radiotherapy and EGFR inhibition in HNSCC” Citron F et al., EMBO Mol Med (2021).

Author contributions:

Lorena Musco has substantially contributed to the experimental work, to analyze and interpret the data.

TABLE OF CONTENTS

ABSTRACT 1

1. INTRODUCTION 4

1.1 Head and Neck Squamous Cell Carcinoma 5

1.2 microRNA in HNSCC 9

1.3 SP/KLFs Factors 11

1.4 TP53 in HNSCC 15

2. AIM OF THE STUDY 20

3. MATERIALS AND METHODS 22

3.1 Cell biology experiments 23

3.1.1 Cell culture 23

3.1.2 Lentiviral transduction of HNSCC cells 23

3.1.3 Cell viability and IC50 drug calculation 24

3.1.4 Sphere-forming assay 24

3.1.5 Luciferase assay 25

3.1.6 Clonogenic Assay 26

3.1.7 Irradiation and survival fraction assay 26

3.1.8 Anchorage-independent soft agar assay 27

3.2 Molecular biology experiments 27

3.2.1 RNA extraction and qRT–PCR analyses 27

3.2.2 Droplet Digital PCR (ddPCR) assay 28

3.2.3 Protein extraction, immunoprecipitation, and western blot analysis 28

3.2.4 Chromatin immunoprecipitation assay 30

3.2.5 Immunofluorescence analysis 31

3.2.6 Histological analysis and immunohistochemistry 31

3.2.7 TUNEL assay 31

3.3 Animal studies 32

3.4 Patient samples and study approval 32

3.5 Statistical analyses 34

4. RESULTS 36

4.1 miR-9 regulates the plasticity of HNSCC-derived cells 37

4.2 miR-9 expression is positively regulated by EGFR activation 39

4.3 miR-9 regulates the response to radiotherapy, but not to chemotherapy, in HNSCC cells 41

4.4 miR-9 regulates the response to RT+CTX, also *in vivo* 44

4.5 miR-9 positively regulates SP1 expression 47

4.6 miR-9 indirectly regulates SP1 expression by targeting KLF5 49
4.7 TP53 status in HNSCC dictates different KLF5 impact on SP1 expression 52
4.8 KLF5/p53/SP1 axis modulates response to therapy of HNSCC, *in vitro* 55
5. DISCUSSION 58
6. REFERENCES 63
AKNOWLEDGEMENTS 73

ABSTRACT

Head and Neck Squamous Cell Carcinoma (HNSCC) represents the sixth most common cancer worldwide, with only the 40-50% of patients surviving at five years from diagnosis. HNSCC can be classified as negative or positive for human papilloma virus (HPV) malignancies, which greatly differ for pathological, molecular features and clinical outcome.

TP53 mutations are the most frequent genetic alteration in HPV-negative HNSCC, playing an uncontested role in its pathogenesis. On the contrary, HPV-positive HNSCC are mostly TP53 wild type and usually less heterogenic, displaying a more favorable prognosis compared to HPV-negative ones. Radiotherapy (RT) *plus* the anti-EGFR monoclonal antibody Cetuximab (CTX) may represent an effective combination therapy for a subset of HPV-negative/TP53 mutated HNSCC patients. However, prognostic/predictive markers of efficacy are missing, resulting in many patients treated with disappointing results and unnecessary toxicities.

Several microRNAs (miRs) are dysregulated in HNSCC and we have recently identified a 4-miR-signature identifying HNSCC patients at high risk of developing recurrence. Among the 4, miR-9 was linked to epithelial to mesenchymal transition (EMT) and progression, and displayed the strongest association with recurrence risk.

By this work, we aimed to study more in detail the role of miR-9 in HNSCC tumor initiating ability, in disease progression and in response to therapies. By this approach, we discovered a new signaling axis involving miR-9, KLF5, SP1, and we investigated its different behaviors depending on TP53 status of HNSCC. We observed that activation of EGFR upregulates miR-9 expression, which sustains the aggressiveness of HNSCC cells and protects from RT-induced cell death. Mechanistically, by targeting KLF5, miR-9 regulates the expression of the transcription factor SP1 that, in turn, stimulates tumor growth and confers resistance to RT+CTX, *in vitro* and *in vivo*. Intriguingly, high miR-9 levels had no effect on the sensitivity of HNSCC cells to cisplatin. In primary HNSCC, miR-9 expression correlated with SP1 mRNA levels and high miR-9 expression predicted poor prognosis in patients treated with RT+CTX.

We discovered that regulation of SP1 by miR9/KLF5 axis worked differently depending on TP53 status: when p53 was mutated KLF5 downregulated SP1 and miR-9 overexpression inverted this trend; when p53 was wild type, KLF5 led to opposite effects, upregulating SP1 expression and increasing its transcriptional activity. Moreover, down-modulation of KLF5 expression affected the responsiveness to RT+CTX treatment, depending from their TP53 status, re-sensitizing the HNSCC TP53 wild type cells and increasing the resistance of the TP53 mutated ones.

Altogether, this newly identified axis, involving miR-9/KLF5/SP1/p53, not only represents a novel potential prognostic and predictive biomarker for CTX activity that can explain why only a subset of

HNSCC patients benefits from the combined use of RT+CTX, but may also promote the development of new targeted therapeutic strategies for HNSCC patients.

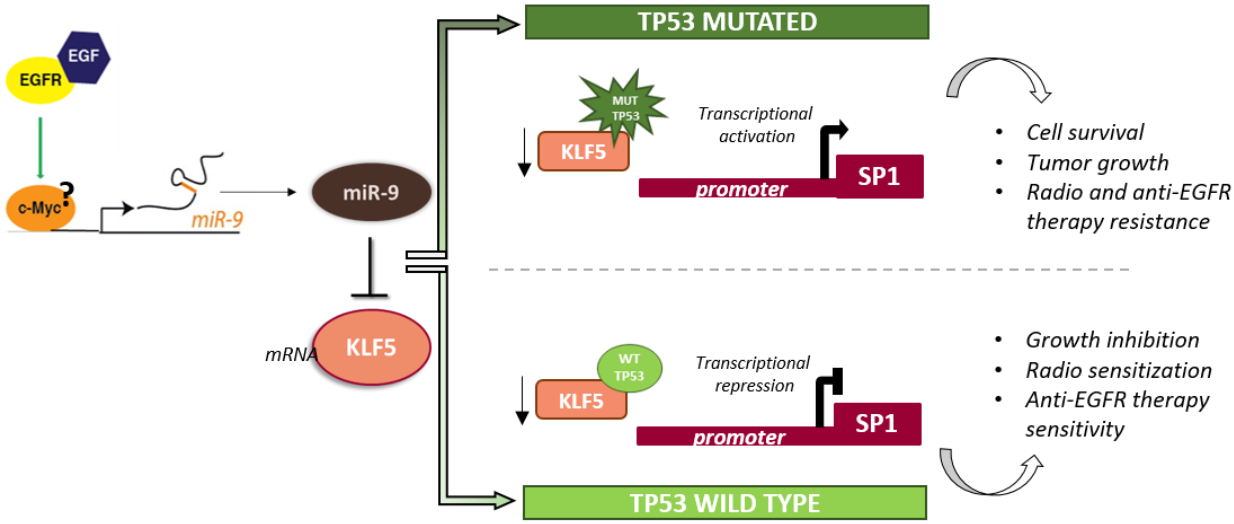

Schematic representation of the putative miR-9/KLF5/SP1/p53 axis. *This graphical model shows the miR-9/KLF5 axis in the regulation of Sp1 promoter depending on TP53 status. The activation of EGFR upregulates the expression of miR-9 that targets the 3'UTR of KLF5 mRNA inhibiting its function. Moreover, down-modulation of KLF5 expression affects cell survival and the responsiveness to Radio and anti-EGFR therapy, depending on the TP53 status, re-sensitizing the HNSCC TP53 wild type cells and increasing the resistance of the TP53 mutated ones.*

1. INTRODUCTION

1.1 Head and Neck Squamous Cell Carcinoma

Head and Neck Squamous Cell Carcinoma (HNSCC) arises from the mucosal epithelia of the upper aero digestive tract and comprises several solid tumors originating from the squamous epithelium of lips, oral cavity, hypopharynx, oropharynx, nasopharynx and larynx [1] (Fig. 1).

HNSCC represents the sixth most common cancer worldwide, with approximately 890,000 new cases and 450,000 deaths/year worldwide. Unfortunately, only the 40-50% of patients will survive five years post-diagnosis [2].

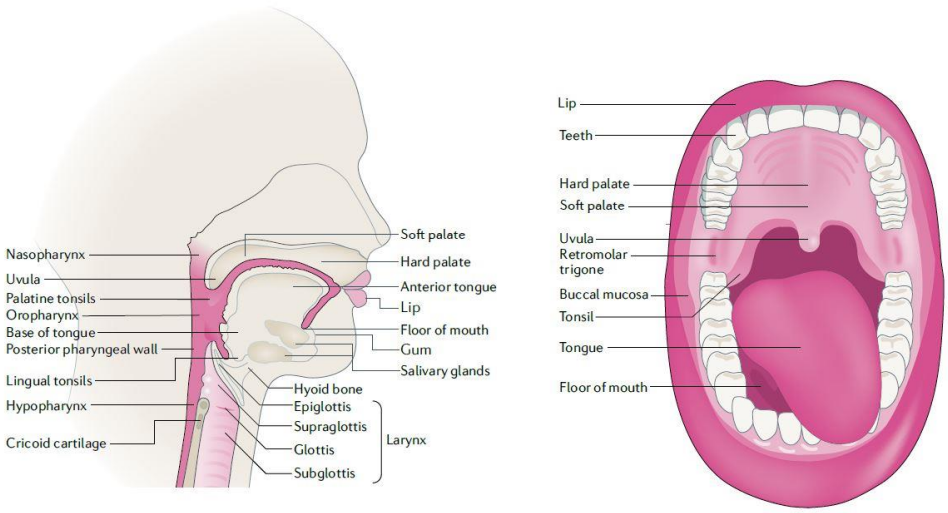

Fig. 1: Anatomical sites of HNSCC development. *Head and neck squamous cell carcinoma (HNSCC) arises from the mucosal epithelium of the oral cavity (lips, buccal mucosa, hard palate, anterior tongue, floor of mouth and retromolar trigone), nasopharynx, oropharynx (palatine tonsils, lingual tonsils, base of tongue, soft palate, uvula and posterior pharyngeal wall), hypopharynx and larynx. Figure has been adapted from "Head and neck squamous cell carcinoma", Johnson et al., [3].*

Based on etiological factors**,** HNSCC can be stratified in Human Papilloma Virus -negative (HPV−) or -positive (HPV+) malignancy, differing not only for pathological and molecular features, but also for the clinical outcome [4]. HPV− subgroup comprehends the 80% of all HNSCCs and are generally more frequent in the adult (>60 years) male population. The most important risk factors so far identified are tobacco and alcohol consumption, which seem to have also a synergistic effect. In the western world, the incidence of this subgroup of HNSCC has been slowly declining during the last years, which can be attributed to a decrease in the prevalence of risk factors, most notably smoking [1,4]. HPV+ carcinoma, the minor subclass of HNSCC for incidence, is caused by HPV infection and associated with high-risk sexual behaviors. HPV is the pathogenic agent and the viral genome has been observed in about 72% of the cases. Similar to cervical cancers, HPV-16 is the most common subtype that accounted for about 80% infected cases of the HPV HNSCCs encoding for E6 and E7 viral proteins. TP53 and RB1 gene mutations were rarely detected in HPV HNSCCs [5,6,7] . However, HPV-16 E6 and E7 viral proteins induce cellular transformation and prevent apoptosis inhibiting the

activity of tumor suppressor p53 and retinoblastoma 1 protein, respectively [8] (Fig. 2). HPV+ carcinomas affect in prevalence tongue and oropharynx and has the same frequency in men and women, with an earlier onset [9].

HNSCCs manifest high levels of heterogeneity, as well as disparities in therapeutic response. Among HPV− early lesions, there is a marked inter- and intra-tumor genomic variability. In this context, *TP53* mutations are the most frequent genetic alteration, detectable in about 85% of HPV− HNSCC patients, playing an uncontested role in pathogenesis of these HNSCC, even though it cannot be considered a univocal prognostic marker [10,11]. Also, *EGFR*, *CCND1*, *PIK3CA* and *MET* amplifications, occurring in HPV− tumors, are considered frequent events in early lesions, as well as inactivation of important onco-suppressor genes, such as *CDKN2A*, *RB1*, *PTEN* and *NOTCH*. In late stages of HPV− diseases, alterations in *E-Cadherin*, *VEGF*, *PDGF* and *TGFb* signalling, are quite frequent and contribute to a worse prognosis [4,12,13].

Regarding HPV+ lesions, most of them are *TP53* wild type and usually less heterogenic and, overall, display a more favorable prognosis compared to HPV− HNSCC.

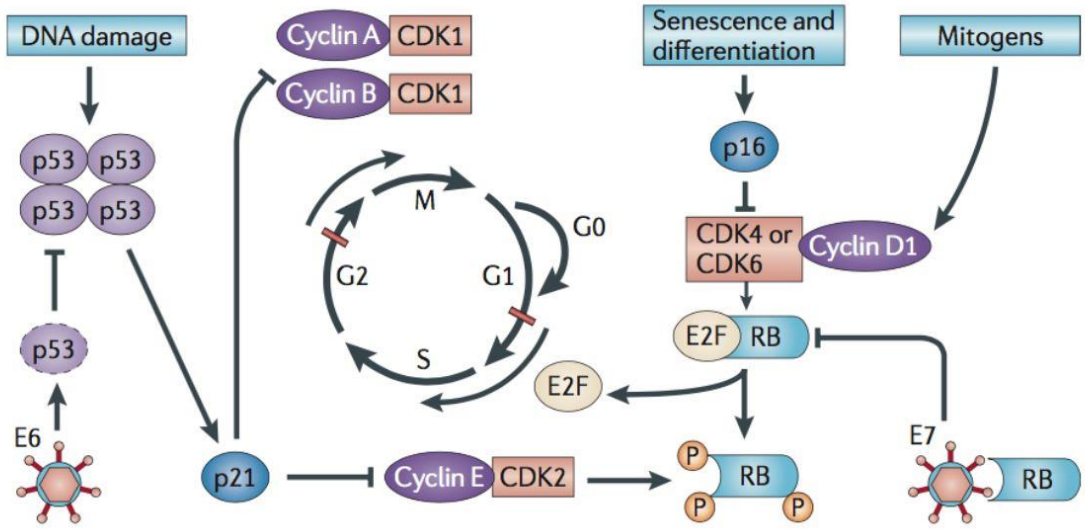

***Fig. 2: Cell Cycle dysregulation by HPV infection**. This schematic representation of cell cycle principal effectors shows the G1/S and the G2/M checkpoints (red bars). RB pocket proteins and p53 respectively mainly control these two important steps. RB proteins normally bind to and inactivate E2Fs transcription factors, which induce the expression of S phase genes. The key protein p53, once activated by phosphorylation, acts as a stress-induced transcription factor leading to p21CIP expression that in turn inhibits several cyclin-CDK complexes leading to cell cycle arrest. HPV genome encodes for two viral onco-proteins: E6 and E7. The E6 protein binds p53 and targets it for degradation, whereas the E7 protein binds to inactivate RB pocket proteins. The molecular consequences of these viral onco-proteins expression are cell cycle entry and inhibition of p53-mediated apoptosis, which allows the virus to replicate. During the HPV infection, the expression of E6 and E7 is not confined to the differentiating layer of the squamous epithelium, but it is detectable also in the basal layer, where stem cells reside leading to the abrogation of the cell cycle checkpoints and virions production. Figure has been adapted from "The Molecular Biology of Head and Neck Cancer", Leemans et al [1].*

However, independently from the etiological agents, HNSCC is a heterogeneous disease and its progression is a stepwise process, resulting from the accumulation of molecular alterations in the

squamous epithelium, which eventually drive the progression from premalignant lesions to invasive disease (Fig. 3).

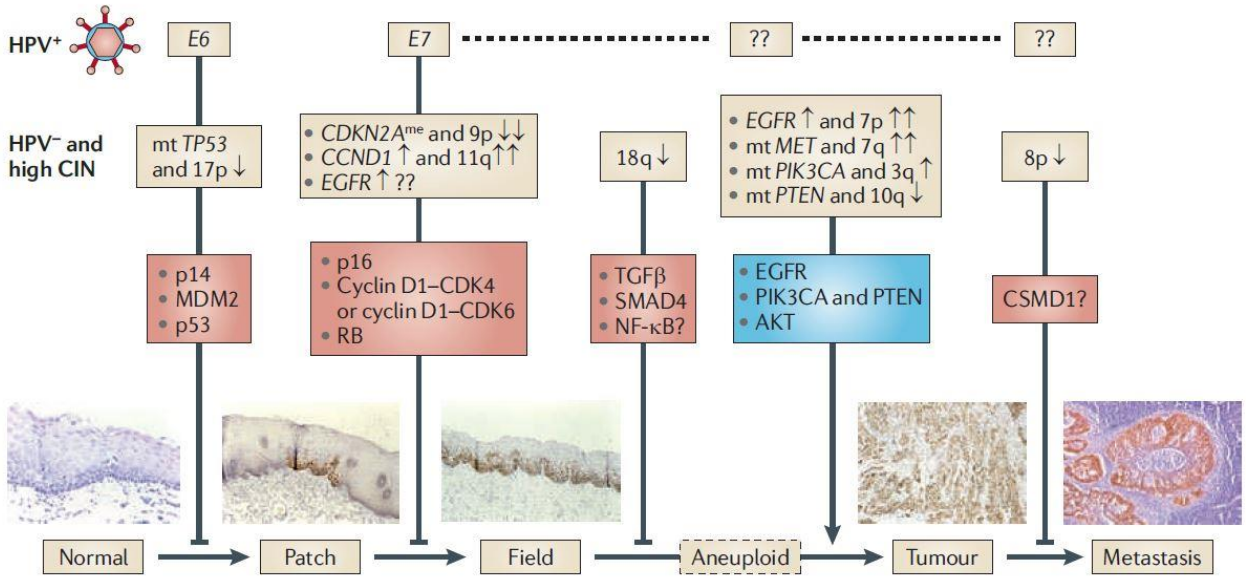

***Fig. 3*: Schematic representation of molecular carcinogenesis of HNSCC.** *A progenitor or adult cell in the normal mucosa acquire one (or more) genetic alteration, including TP53, either by mutation (HPV negative) or by inhibition (HPV positive). Also, CDKN2A tumor suppressor gene is inactivated in early stages while the accumulation of other mutations in PTEN, EGFR, PI3KCA genes occurs at later stages turning the field to an overt carcinoma with invasive growth and metastasis capabilities. Figure has been adapted from "The Molecular Biology of Head and Neck Cancer", Leemans et al* [1].

The prognosis of HNSCC patients is largely determined by the stage at presentation, which comprehends an evaluation of the extent of the tumor, the presence of lymph-node invasion and distant metastases. The tumor stage of HNSCC is defined by clinical examination, with the integration of imaging, cytology of lymph-nodes and tumor histopathology after surgery (such as radicality and extra-nodal spread) [1].

Early-stage tumors (stage I/II), representing the minor part of the cases, are treated with surgery or radiotherapy alone and have a favorable prognosis, while the mainstays of treatment for advanced tumors (stage III/IV) are surgery combined with postoperative chemo- and/or radio-therapy [3].

The standard treatment for advanced patients is the administration of Cisplatin (CDDP), as radio-sensitizing agent, 100 mg/m2 once every three weeks, *plus* radiotherapy [14,15]. However, to overcome the highly toxic side effects of Cisplatin, this schedule can be adapted to a decreased dose administered once a week, or modified by the use of Carboplatin or Paclitaxel [16].

Although this combination of chemo- and radio-therapy is considered the most valid, although highly toxic, therapeutic strategy, the 5-year survival of HNSCC patients is still very low, ranging from 35 to 55%. This trend has not markedly improved in recent decades, mostly due to the aggressive and

invasive growth pattern as well as high resistance against available therapies, leading to loco-regional relapse and/or distant metastasis [3,17]. The limited information available on the molecular carcinogenesis of HNSCC and these features of genetic and biological heterogeneity has hampered the development of new therapeutic strategies [4,5].

As mentioned above, over 90% HPV− HNSCC early lesions display an overexpression of EGFR that can be detected by IHC [18]. This observation, together with the notion that a positive regulatory loop exists between EGFR and Cyclin D1 transcription [19], supported the hypothesis to develop new therapeutic strategies involving the combined treatment with targeted- and standard chemo- or chemo/radio-therapy [20]. In this context, Cetuximab (CTX), an epidermal growth factor receptor inhibitor approved by the US Food and Drug Administration, showed a reduced toxicity compared with standard RT+CDDP and might thus represent a viable way to de-escalate treatment for HNSCC patients. Cetuximab is a chimeric IgG1-subclass monoclonal antibody that binds to the extracellular domain of the EGFR with higher affinity than its natural ligands, EGF and TGFα, blocking the activation of its intracellular domain and the subsequent tyrosine kinase-dependent signal transduction pathway [21]. CTX also stimulates the internalization of EGFR, removing the receptor from the cellular surface and thus preventing its interaction with the ligands [22].

Several preclinical studies demonstrated that inhibition of EGFR by CTX increases the efficacy of radiotherapy (RT) [20,23], likely decreasing the proportion of cells in S phase and increasing those in G1 phase, facilitating apoptosis, decreasing DNA repair activity, and inducing an antiangiogenic effect [21].

Definitive radiotherapy (RT) is a standard-of-care treatment for loco regional advanced HNSCC although it is often combined with chemotherapy for systemic treatment. Several phase III randomized trials showed encouraging results comparing the efficacy of definitive radiotherapy (RT) and radiotherapy plus Cetuximab (RT *plus* CTX). In particular, the administration of Cetuximab 400 mg/m2 loading dose, followed by 250 mg/m2 weekly for 8 planned doses, designed to overlap the planned ~7 weeks of radiotherapy or 7 weeks of radiotherapy alone, demonstrated a significant improvement in terms of overall survival especially for HPV− HNSCC patients [21, 24].

Among HNSCC patients, those with HPV+ oro-pharyngeal cancers have a particularly good prognosis and represent a population in which de-escalation treatments would be strongly needed. However, very recent trials demonstrated that in low-risk HPV+ HNSCC patients CTX plus RT is inferior to the standard CDDP regimen, suggesting that in these patients de-escalation to reduce the toxicity of platinum is not feasible with the use of CTX and that HPV infection is not a biomarker of CTX response [25,26]. On the contrary, in HPV− HNSCC patients that, among other things, are the ones that most frequently display EGFR overexpression and *EGFR* amplification, the combination of

radiotherapy plus Cetuximab (RT+CTX) might be equally effective and less toxic than chemoradiotherapy.

1.2 microRNA in HNSCC

MicroRNA (miRNAs or miR) are small non-coding RNA molecules (20-25 nucleotides) that regulate, in a canonical manner, post-transcriptional gene expression through a non-specific binding to the 3'- untranslated region (3'-UTR) of mRNA target [27]. Their sequences are located within various genomic context. While the majority of canonical miRNAs are encoded by introns of non-coding or coding transcripts, and by exon regions, some miRNA genes reside in the introns of protein-coding genes and, thus, share the promoter of the host gene [28]. However, several miRNA genes may have multiple transcription start sites and, thus, the promoter of intronic miRNAs are sometimes distinct from the promoter of their host gene [29].

The canonical biogenesis pathway is the dominant pathway by which miRNAs are processed. The transcription of primary miRNA (*pri-miRNA*) is carried out by RNA-polymerase-II and its associated co-factors that leads to the formation of about 1 kb-long *pri-miRNA,* containing different stem-loop sequences in which the mature miRNA sequence is embedded [30]. Once pri-miRNAs are transcribed from their genes they are processed into *pre-miRNAs* by the microprocessor complex, consisting of an RNA binding protein (DGCR8) and a ribonuclease III enzyme, Drosha, that crops the stem-loop to release a small hairpin-shaped RNA of about 65-75 nucleotides in length (pre-miRNA) [31,32].

Following the cleavage, pre-miRNAs are exported to the cytoplasm by an exportin 5 (XPO5)/RanGTP complex and then processed by the RNase III endonuclease, Dicer, that removes the terminal loop, releasing a small double strand RNA (dsRNA) [33]. This small RNA duplex is loaded into the Argonaute (AGO) family proteins (AGO1-4 in humans) in an ATP-dependent manner, forming an effector complex named RNA-induced silencing complex (RISC), that rapidly removes the less stable *passenger* strand, eventually releasing the *leading* strand of the mature miRNA [34] (Fig.4).

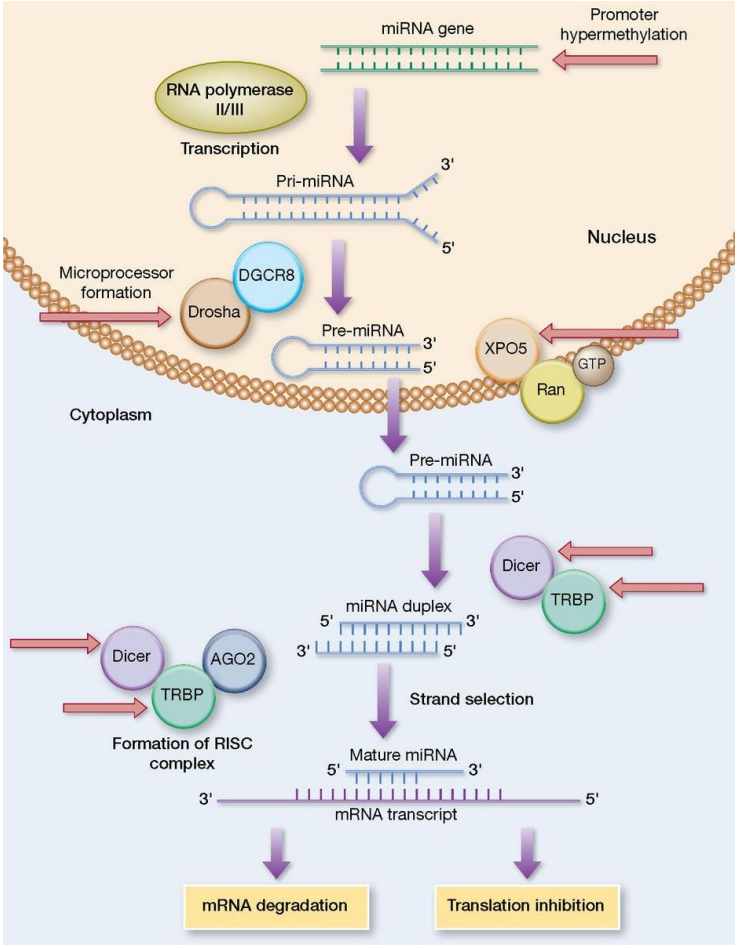

Fig. 4: microRNA biogenesis pathway. *Schematic representation of miRNA biogenesis showing the principal effectors of transcription and maturation processes. The complex regulation of miRNA expression is perturbed in almost all biogenesis step (as indicated with the red arrows) by genetic, and more frequently, epigenetic factors. Figure has been adapted from "miRNA Dysregulation in Breast Cancer" Mulrane et al* [35].

Each miRNA has two possible mechanisms of action based on the degree of complementarity between the miRNA seed sequence and its mRNA target. First, if the target mRNA and miRISC have a perfect base pairing, the mRNA is cleaved and degraded through activation of the RNA-mediated interference pathway. On the contrary, and more commonly, the imperfect pairing between a miRNA and its target results in translation inhibition or repression due to the formation of mismatched 'bulges' in the central region of the miRNA [36]. Different evidences reveal that miRNA:mRNA interaction can occur through the canonical direct binding to the 3'UTR and also through a non-canonical binding to either the coding sequence or the 5'UTR [37]. For this reason, the identification of the broadness of miRNA:mRNA interaction remains an open challenge and a possible field of investigation in different pathologies, including cancer.

Another way miRNA can exert their function is by the recruitment of transcriptional factors in the nucleus, driving them to their correct gene promoters. Tightly depending on cell state, nuclear

miRNAs can enhance the transcription of different genes, leading to an increase of their translation, unhinging the common mechanism whereby miRNA activity results in a down-modulation of its target(s) [38,39].

miRNAs regulate approximately 30% of human genes both up- or down-regulating different target genes and indirectly acting as oncogene or oncosuppressor gene [40]. They are specifically expressed in diverse tissues and biological fluids, and particular miRNAs pattern are characteristic of different cell types and function. Moreover, they are involved in essential biological activities and cellular processes, including the regulation of cell cycle, proliferation, differentiation, development and apoptosis and also cell plasticity and cancer development [30,41]. MicroRNA expression is widely altered in tumors, and their deregulation has been used for diagnosis as well as to predict relapse, survival and response to therapies [42,43].

In HNSCC, several miRs are differentially expressed with respect to the normal/ peritumoral mucosa [44,45]. Few years ago, it was discovered by our lab that a four-miR signature (miR-1, miR-9 miR-133, and miR-150) efficiently identifies HNSCC patients at high risk of developing loco-regional recurrence targeting the epithelial to mesenchymal transition (EMT) process and impacting on HNSCC response to therapies and on progression [46]. Among the four miRs of the signature, *miR-9* displayed the strongest association with recurrence risk [47]. In line with these findings, other studies reported that miR-9 is overexpressed in the saliva of HNSCC patients, in the cancer stem cell population, and that it correlates with invasion and metastasis in a mouse model of SSC [48,49].

1.3 SP/KLFs Factors

Specificity Proteins (SP) and Krüppel-like factors (KLFs) are collectively referred to as the SP/KLF family of DNA-binding transcriptional regulators, which bind with varying affinities to DNA sequences called ‘SP1 sites’ (e.g. GC-boxes, CACCC-boxes, and basic transcription elements) and share a mostly nuclear localization [50].

From the identification of the first member of the SP/KLF family, SP1, in 1983, human genes encoding for 17 KLFs and 9 SP have been identified [51] (Fig. 5).

A structural level, SP/KLFs proteins have a high conservative triple Cys2/His2 zinc-finger DNA-binding domain at the carboxyl terminus, very important for the transcriptional activity, but other regions can be highly divergent. The main difference distinguishing SPs from KLFs is the absence of a Buttonhead (Btd) box CXCPXC preceding the triple zinc finger region in the latter [52]. The divergence at the N-terminus also permits the binding to different co-activators, co-repressors or other

cofactors, including histone-modifying enzymes, resulting in additional functional diversity [53,54] (Fig.5).

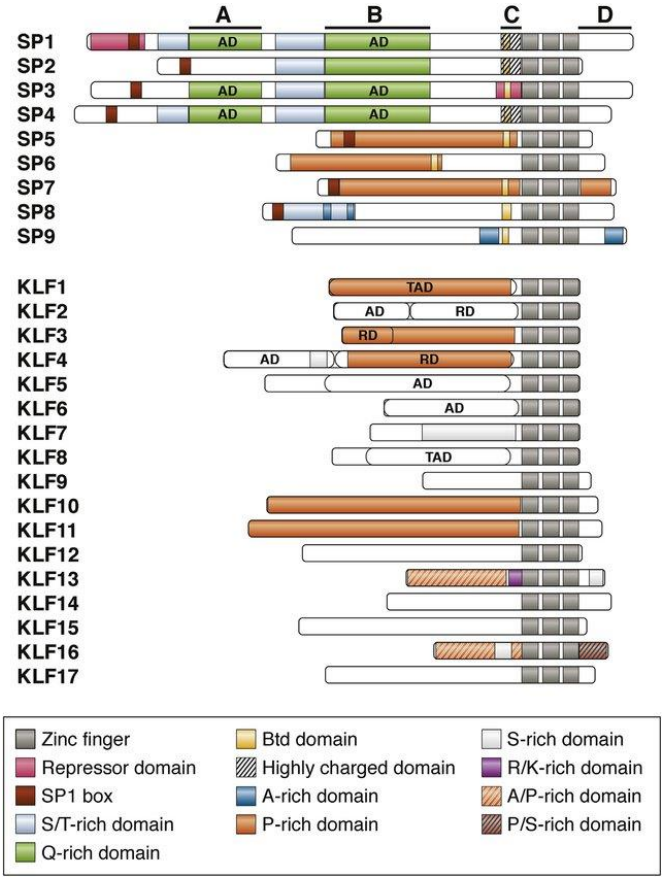

Fig. 5: Structure of human SP and KLF proteins*. This schematic representation shows that the 9 SP and the 17 KLF proteins share at the C-terminus the same triple zinc finger domain (in grey). The* ***A****,* ***B****,* ***C****, and* ***D*** *define the modules of SP1, while at the N-terminus there are the Activation, Repression, and Transactivation Domains (AD, RD, and TAD, respectively) that can be highly divergent giving to these Sp-KLFs factors additional functional diversity. Figure has been adapted from "SP and KLF Transcription Factors in Digestive Physiology and Disease", Kim et al.*[51].

SP/KLFs factors are involved in many growth-related signal transduction pathways and their overexpression can have either positive or negative effects on proliferation, differentiation and migration, depending on the cellular type [55]. These proteins have also been implicated in cancer onset and progression, interacting with oncogenes and tumor suppressors or being oncogenic themselves [53,56]. Moreover, they have several context-dependent functions, partly mediated by different molecular switches, such as p53, p21, SIN3A, Notch [57,58]. Alternative splicing, post-translational modifications, including SUMOylation, acetylation, ubiquitination, and phosphorylation, impact on the stability and activity of these proteins [59]. Different family members can have very different transcriptional properties and also modulate each other's activity by a variety of mechanisms, since their own promoters all contain the "SP1 sites" [50].

Sp factors, which all have the Btd box CXCPXC preceding the triple zinc finger unlike the KLFs factors, are typically divided into 2 groups based on the structural features. SP1, SP2, SP3, and SP4

(Group 1) share a similar modular structure. SP1, SP3, and SP4 contain two major glutamine-rich transactivation domains (TD) close to serine/threonine-rich sequences that may be a target for post-translational modification. Compared to the others, SP2 has only one transactivation domain with a different consensus-binding site in zinc finger.1. With the exception of the Btd and the SP boxes, the N-terminal regions of SP5, SP6, SP7, SP8 and SP9, belonging to the Group 2, are completely different from those of the Group 1 and more closely related to each other. However their biochemical and molecular properties have not been studied deeply, yet (Fig. 5?) [50,51,60].

Specificity Protein 1 (SP1) was the first mammalian transcription factor to be cloned in 1980s. It is ubiquitously expressed and involved in basal transcriptional regulation of several genes related to many cellular processes, including cell differentiation, growth, apoptosis, immune response, DNA damage repair, chromatin remodeling and also tumorigenesis [53,61]. Indeed, it is over-expressed in a number of neoplasia, including breast, gastric, pancreatic, lung, brain (glioma) and thyroid cancers and in most cases, SP1 levels correlate with stage, invasive potential, metastasis stem-ness chemo resistance and thus, with poor prognoses [62,63]. SP1 activity is regulated by post-translational modifications such as phosphorylation, acetylation, glycosylation, and proteolytic processing that can positively and negatively influence DNA binding and thus, its transcriptional activity depending on the regulatory factors and on the domain that these modify.[64,65]. For example, cyclin A-CDK mediated phosphorylation increases the DNA-binding activity of SP1 [66], while Pin1-mediated SP1 phosphorylation by CDK1 decreases its DNA-binding activity during mitosis [67]. Moreover, ataxia telangiectasia mutated (ATM) kinase, activated during DNA damage, hyper-phosphorylates SP1 at Ser101 that increases its expression at sites of double-strand breaks interfering in DNA damage response pathway [68]. Apart from members of the SP/KLFs factors, SP1 can recruit and form complexes with other transcription factors and can switch its activity interacting with them, either directly or indirectly (TBP, TAF proteins, Rb, YY1, E2F, CRSP, FBI-1, p300, HAT, HDAC, p53). These interactions have proved to be crucial in the regulation of many cellular functions by transcriptional control of both housekeeping genes and of a complex of genes with distinct roles in development and homeostasis of many tissue types [69,70].

With regard to the currently known 17 human KLF proteins, they can be divided into three distinct groups, based on functional and structural characteristics. KLFs in Group 1 (KLF3, 8, and 12) act as transcriptional repressors through their interaction with the C-terminal binding protein (CtBP) [71,72]. KLF1, 2, 4, 5, 6, and 7 (Group 2) function predominantly as transcriptional activators binding to acetyl-transferases, such as CREB binding protein (CBP), p300, and p300/CBP-associated factor [71,73]. On the contrary, KLF in Group 3 (KLF9, 10, 11, 13, 14, and 16) have repressor activity through their interaction with the common transcriptional co-repressors, such as Sin3A, CtBP1 and CtBP2, which

in turn recruit HDACs, methyltransferases and other silencing complexes [74]. KLF proteins are highly conserved among mammals from human to rat and their expression varies depending on the cellular and tissue type. Some family members are expressed ubiquitously (*e.g.* KLF6, 10, and 11), whereas others are tissue-specific, such as KLF1and KLF2 that are expressed predominantly in erythroid cells and T-lymphocytes or KLF4 and KLF5 that are very abundant in the gastrointestinal tract [75,76].

The structural homology in their carboxyl-terminal zinc finger domains creates overlap in KLF transcriptional targets; as an example, in ES cells, KLF2, 4, and 5 can all bind and activate Esrrb, Fbxo15, Nanog, and Tcl1. However, the distinct amino-terminal sequences provide unique regions for interaction with specific and different binding partners [50,53].

Beside the roles of KLFs in normal cells and tissues, several tumor suppressive and oncogenic functions have been proposed for these proteins in different human cancers [56,58].

Human Krüppel-like factor 5 (KLF5, also known as BTEB2 and IKLF) was first identified as intestinal-enriched Krüppel like factor (IKLF) due to its predominant expression in the epithelial crypt cells of the gastrointestinal tract [57,77]. It is involved in regulating expression of a broad range of genes, and thus affects different cellular functions, such as stem cell self-renewal, cell proliferation, differentiation, and apoptosis [78]. Typically, KLF5 is pro-proliferative in normal cells and in many human cancers, including breast, intestinal, colon, bladder, leukemia, cervical cancers etc. [79,80]. Through interactions with other proteins, such as CBP/P300 or NF-κB, in different cell systems, KLF5 is able to induce the expression of different genes, including smooth muscle cell differentiation marker SM22α, cyclin D1, PDGFa and also transforming growth factor β (TGF-β) [71,81,82].

Moreover, during the last few years, several studies have demonstrated that KLF5 plays a crucial role in the response to therapy, in different tumoral context [79]. In particular, it can confer resistance to chemotherapies by upregulation of survivin or HIF1α [83,84] or it may modulate DNA repair pathways preventing intestinal injury induced by total body radiation, in mice [85].

Loss of KLF5 promotes apoptosis through Pim1 kinase, conferring colon cancer cell sensitivity to DNA-damaging agents [85]. In breast cancer KLF5 expression is often associated with poor patient outcome [86,87], especially in the HER2-enriched subtype since it suppresses the therapeutic response to HER2 inhibition, inducing the anti-apoptotic activity of MCL1 and BCL-XL factors [88].

However, in head and neck squamous cell carcinoma and prostatic cancer, KLF5 acts as a tumor suppressor, inhibiting cancer cell survival and invasion [59,78,86].

As a member of the SP-KLF protein family, also KLF5 has several context-dependent functions [59]. An altered genetic background, for example the presence of oncogenic Ras, can lead to phosphorylation of KLF5 by extracellular signal-regulated kinase (ERK), inversing the functioning of the protein that loses its proliferation promoting effect, typical for normal intestinal crypt cells [56,89].

A similar effect was observed in normal keratinocytes under TGFß treatment, suggesting that Ras-transformed cells have acquired an intrinsic competence to modulate KLF5 functions, whereas normal cells need the extrinsic influence from the TGFß cytokine [90].

Post-translational modification of KLF5 also modulates its function. SUMOylation of KLF5 facilitates its nuclear localization and enhances anchorage-independent growth in colon cancer cells [91]. Acetylation instead alters the function of KLFs on target genes. For example, non-acetylated KLF5 fails to activate CDKN2B, but, upon TGFβ stimulation, KLF5 is acetylated by p300 and induces transcription of CDKN2B, resulting in reversal of KLF5 function with growth inhibition [92,93].

Another important molecular switcher of KLF5 activity is TP53. In non-transformed human primary esophageal keratinocytes, when p53 is wild type, KLF5 plays a pro-proliferative role, while it becomes anti-proliferative when p53 is mutated. KLF5 loss in human primary keratinocytes harboring p53 mutation accelerates the cell cycle decreasing expression of p21Waf1/Cip1 whose promoter is bound and differently regulated by KLF5 depending on p53 context [94,95].

Moreover, also in transformed intestinal and esophageal cancer cells, KLF5 seems to show a p53 context-dependent function. During esophageal squamous cell transformation, it transactivates Notch1 when p53 is mutated so KLF5 loss limits Notch1 activity transforming human keratinocytes and leading to the formation of invasive tumors [96].

Thus, based on these evidences, changes in p53 status could be key for the context-dependent effects of KLF5.

1.4 TP53 in HNSCC

One of the main "molecular switches" mediating SP1/KLFs protein functions is p53, the major tumor suppressor mutated in over half of all human cancers.

p53 (encoded by the gene TP53 in humans) functions primarily as a transcription factor, which, upon cellular stress signals, regulates a great amount of genes promoting cell cycle arrest, senescence, apoptosis, differentiation, DNA repair and other cellular and molecular processes [97, 98] (Fig. 6).

Accordingly, p53 function is usually compromised in tumoral cells, mainly due to somatic mutations, which occur in the majority of human cancers and constitute a cornerstone in tumorigenesis. The frequencies of reported TP53 mutations vary considerably between cancer types, ranging from ~10% for example, in hematopoietic malignancies [99] to 50–90% in ovarian colorectal and head and neck squamous cell carcinomas [100,101,102]. While somatic TP53 mutations lead to sporadic cancer, germline TP53 mutations cause a rare type of cancer predisposition known as Li–Fraumeni Syndrome [103].

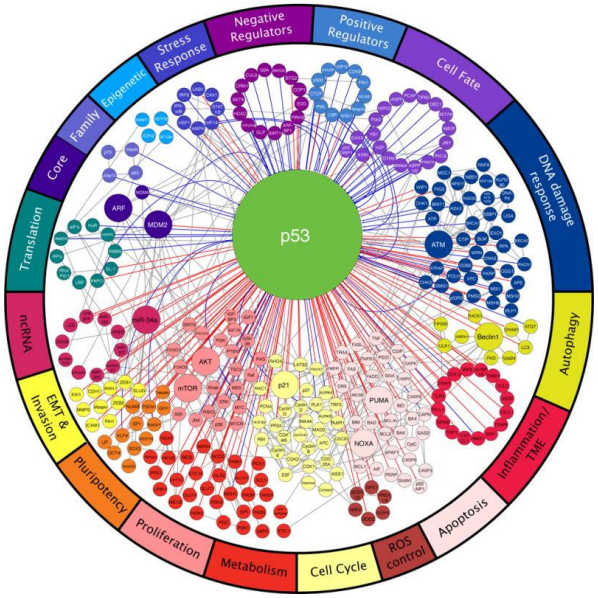

***Fig. 6: The p53 Network**. A wide variety of regulators interferes with the activity of p53 that, in turn, controls many distinct biological processes. Each node represents a gene and each line represents an interaction. Direct p53 inputs are indicated as blue lines and direct p53 outputs are indicated as red lines. Noticeably, p53 controls effector processes by activating multiple target genes. Downstream pathways are highly interconnected. Figure has been adapted from "Putting p53 in Context" Kastenhuber, E,* [109].

Approximately 80% of these mutations are missense mutations in its DNA-binding domain that result in the formation of a stable full-length mutant protein that has lost its sequence specific DNA-binding activity and that, therefore, is unable of activating p53 target genes and suppressing tumorigenesis. Almost one third of all missense mutations arise in six hotspot residues [104] (Fig. 7).

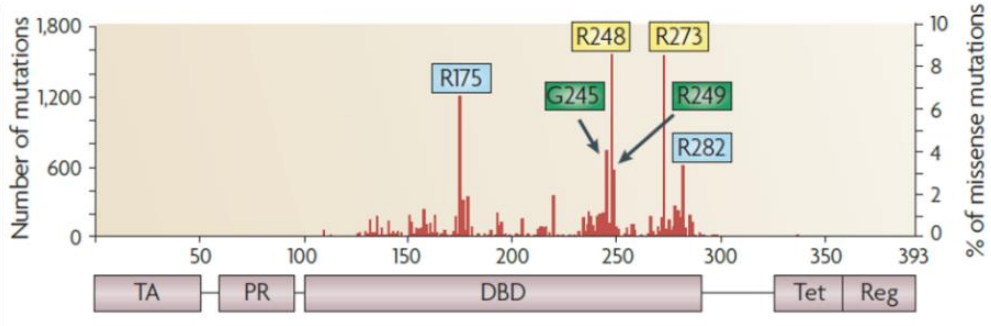

***Fig. 7: Distribution of TP53 somatic mutations**. The graph represents the distribution of the missense mutations along the 393 amino-acid sequence of p53. The six most common hotspot mutations are highlighted in yellow for DNA-contact mutations, green for local conformational mutations and blue for global conformational mutations. They are clustered within the central most conserved region of p53, the DNA-binding domain, (DBD).In addition to the DBD, the p53 sequence contains also the Transactivation domain (TD), Proline-Rich domain (PR), Tetramerization domain (Tet) and Carboxy-terminal Regulatory domain (Reg). Figure has been adapted from "When mutants gain new powers: news from the mutant p53 field"* [105].

Besides losing their wild-type activities, many p53 mutants also function as dominant-negative proteins that inactivate wild-type p53 expressed from the remaining wild-type allele. Moreover, some mutant p53 forms also acquire new oncogenic properties that are independent of wild-type p53, known as 'gain-of-function' (GOF) properties [105].

Recent findings broaden the array of GOF properties and highlight their relevance to tumorigenesis. In particular, p53 mutants are able to bind transcriptional factors (TF) and transactivate or attenuate target gene expression through preferential binding to other structural DNA motifs and not consensus sequences. Mutant p53 may also function to increase chromatin accessibility driving the expression of genes within distinct regions of the genome [106, 107].

The different p53 missense mutations generate p53 mutant proteins with varied conformations and binding affinities, resulting in different spectra of transactivated or inactivated target genes and variations in cellular phenotypes. Indeed, within cells of a particular histologic identity, different mutant p53 proteins may therefore drive different biologic behaviors. However, it is intriguing that many different p53 missense mutations, within the p53-binding domain, nonetheless regulate identical effector proteins and target genes [108, 109].

Mutant p53 can bind to and cooperate with transcription factors, such as p63, p73, nuclear factor-κB, NF-Y, E2F1, VDR, SP1, SREBP, and ETS, to enhance or repress targets gene expression. It can also engage in epigenetic regulation of chromatin remodeling via the SWI/SNF complex and chromatin regulatory proteins methyltransferase MLLs and acetyltransferase MOZ [105,110].

In this way, p53 mutants interfere with most of the biological pathways leading to tumor initiation and progression (Fig. 8).

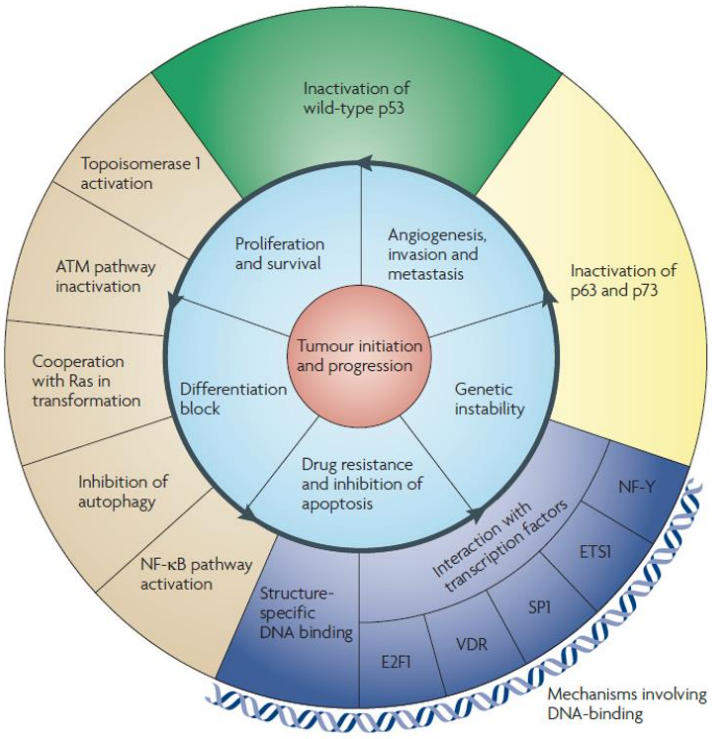

Fig. 8: Oncogenic properties of mutant p53 and their underlying mechanisms*. The outer circle depicts key properties of p53 mutants: inactivation of wild-type p53, p63 and p73, interaction with transcription factors or structure-specific DNA binding, interference with other several pathways (autophagy, DDR pathway ecc.) These properties underlie the oncogenic phenotypes listed in the inner circle (shaded blue) that lead to tumor initiation and progression. Each of the phenotypic effects can be attributed to almost each of the mechanistic properties; hence, the inner blue circle can be freely rotated. Figure has been adapted from "When mutants gain new powers: news from the mutant p53 field"* [105]

The abrogation of p53 function through mutations in its gene or interaction with viral proteins is one of the most common molecular alterations in HNSCC and represents an early event in the progression of this tumor [4].

TCGA analysis results demonstrated that more than 70% of head and neck tumors have TP53 mutations. In particular, tumors of the larynx and hypopharynx have the highest TP53 mutation rate (83.5%), while tumors of the oropharynx, including the tonsils, and base of the tongue have the lowest TP53 mutation rate (28.6%) because the majority of oropharyngeal cancers are HPV-associated [111].

Although the spectrum of TP53 missense mutations is wide, the missense variants within codons R248, R273, G245, R175, R282, and H179, are the most prevalent hotspot mutations in HNSCCs [112].

Very recently, scientific evidences demonstrated that metastatic HNSCC is characterized by a lower frequency of TP53 mutations compared to primary tumor possibly due to the high metastatic potential of HPV+ oropharyngeal and nasopharyngeal tumors that harbor TP53 mutations with a lower frequency [100].

However, the mutational spectrum of TP53 varies in its prognostic power that has not been clearly established, and by itself is not sufficient for the development of the human HNSCC.

Insights into the different effects of p53 missense mutations are critical also for the development of HNSCC cancer prevention and therapeutic strategies. Also in this tumor context, in fact, mutant p53 GOF is the product of functional partnerships between mutant p53 proteins and available interacting proteins that together mediate changes in cell phenotypes through altered gene expression [109].

Among the proteins that interact and cooperate with p53 in gene regulation, there are many belonging to the SP/KLFs family. Moreover, the different “SP1 sites” present in DNA promoters are able to mediate transcriptional effects of both wild-type and mutant p53 and, interestingly, the effects of these two proteins often differ in cancer [50,54,94,113].

For instance, SP1 interacts with wild type p53 as well as with mutated p53 proteins interestingly leading to opposite and antagonistic transcriptional outcomes depending on the status of the p53 protein. While wild type p53 inhibits SP1-dependent activation, presumably by interfering with DNA binding of SP1, mutant p53 elicits co-operative effects and amplify the activating SP1 transcriptional activity [114]. This cooperative transactivation could be due to the physical interaction between p53 and SP1 (or other transcription factors) or to the direct binding to gene promoters [115,116,117].

The different TP53 status can affect the activity of other SP/KLFs factors, such as KLF4 and KLF5 [53]. KLF4 is one of the factors that reprograms differentiated cells to iPS and that is crucial for the barrier function of the skin [118]. In normal keratinocytes, in presence of physiological levels of wild-type p53, p63 directly represses KLF4 by binding to upstream promoter sites. This regulation is subverted by oncogenic mutations of p53 which activate endogenous KLF4 by hijacking p63 to a

different location on its promoter, turning it into an activator of this reprogramming factor [119]. Moreover, KLF4 cooperates with p53 in activating p21 but can also repress p53 transcription by binding to GC boxes in its promoter, eventually leading to oncogenic or tumor suppressor effects depending on a genetic context [120].

KLF5 also cooperates with both the p53 isoforms, wild type and mutated, modulating the activity of several proteins involved in numerous biological processes. Moreover, it can switch its function depending on p53 status [86]. For instance, KLF5 can interact with p53 to induce survivin gene transcription. In particular, it abrogates the p53-regulated repression of survivin increasing the survival of acute lymphoblastic leukemia cells [121]. Mutant p53 acts as a co-factor of KLF5 in binding the PLA2G16 promoter, which activates its transcription and the cancer cell glycolysis. This cooperation establishes a new mutant p53/KLF5-PLA2G16 regulatory axis in pancreatic adenocarcinoma [122]. In hepatocellular carcinoma, in the context of p53 loss, KLF5 regulates epithelial-mesenchymal transition of liver cancer cells, through miR-192 targeting of ZEB2 [123]. In some cases, p53 and KLF5 functions seem to be competitive: p53 and KLF5-binding sites overlap on some target genes. If p53 wild type is favored on some sites, it is often true that, on the same site, KLF5 may be favored when p53 is mutant, or *viceversa*. For instance, in HNSCC, p53 normally binds to Notch1 promoter but it can be replaced by KLF5 when p53 binding is lost in dysplastic tissue, an early event in squamous cell tumorigenesis [58,84,96].

Overall, these evidences confirm a strong link and interference between these SP, KLF and p53 transcription factors, commonly altered in HNSCCs.

Based on all these scientific evidences, we investigate here why p53 loss or mutation is a condition necessary but not sufficient for development of HNSCC and dissect the role of this new mir-9/KLF5/SP1/TP53 axis that may unveil interesting and important insights for identification of novel prognostic/predictive biomarkers and, possibly, therapeutic targets for HNSCC patients.

2. AIM OF THE STUDY

Head and Neck Squamous Cell Carcinoma (HNSCC) represents the sixth most common cancer worldwide, with about 890,000 new cases/year. HNSCC is a highly heterogeneous disease and, based on etiological factors**,** HNSCC can be classified as a Human Papilloma Virus (HPV) -negative or -positive malignancy, differing not only for pathological and molecular features, but also for the clinical outcome. For instance, while HPV-negative HNSCC are mostly TP53 mutated, HPV-positive ones are mostly TP53 wild type.

Most patients are diagnosed with a locally advanced disease and treated with surgery in combination with radiotherapy and/or chemotherapy. This highly toxic schedule is curative in less than half of the cases and only 40-50% of patients will survive at five years post-diagnosis. The development of local or distant recurrences remains the major clinical challenge, since recurrent patients do not have effective therapeutic options.

Radiotherapy (RT) *plus* the anti-EGFR monoclonal antibody Cetuximab (CTX) has a lower toxicity compared to chemotherapy and represents an effective combination therapy for a subset of HPV-negative HNSCC patients. However, there is currently no biomarker able to predict which patients will respond to RT+CTX, resulting in many patients treated with disappointing results and unnecessary toxicities.

Many clinical challenges need to be faced for a better management of HNSCC patients. First, there is the need for the identification of biomarker(s) able to classify high-risk patients and to predict the response of each patient to the different treatment options currently available. Second, there is the need for new druggable targets to better personalize therapy and, eventually, have a better outcome for patients with advanced HNSCC.

In this PhD project, we have dealt with these unmet clinical needs and aimed to investigate the molecular players that drive tumor aggressiveness and resistance to therapies. We have identified a new signaling axis, involving miR-9, KLF5, SP1, that connects the tumor stem-like features of HNSCC to therapies' response in a TP53-dependent manner. In this work, we described a new mechanism possibly explaining why only a subset of HNSCC patients benefits from the combined use of RT+CTX, and propose a new predictive biomarker of therapy response.

3. MATERIALS AND METHODS

3.1 Cell biology experiments

3.1.1 Cell culture

Head and neck squamous cell lines were obtained from ATCC (LGC Standards) except for UMSCC74B and UMSCC1, which were kindly provided by Dr. Thomas Carey (University of Michigan, Ann Arbor, MI). FaDu (HTB-43), CAL27 (CRL-2095), UMSCC1 and UMSCC74B cells were cultured in Dulbecco modified Eagle medium (DMEM, Sigma) supplemented with 10% fetal bovine serum (FBS, Gibco). SCC9 cells (CRL-1629) were cultured in a 1:1 mixture of Dulbecco's modified Eagle's medium (Sigma) and Ham's F12 medium (Sigma) containing 1.2 g/l sodium bicarbonate (Sigma), 2.5 mM l-glutamine (Sigma), 15 mM HEPES (Sigma), and 0.5 mM sodium pyruvate (Sigma) supplemented with 400 ng/ml hydrocortisone (Sigma) and FBS 10%. HNBE cells (PCS-300-010) were cultured in Airway Epithelial Cell Basal medium (ATCC) supplemented with Bronchial Epithelial Cell Growth Kit (ATCC). All the cells were routinely tested to exclude mycoplasma contamination (MycoAlertTM, Lonza) and authenticated by STR analysis in 2018, according to PowerPlex® 16 HS System (Promega) protocol and using GeneMapperTM software 5 (Thermo Fisher) to identify DNA STR profiles.
All *in vitro* studies were performed in triplicate, unless otherwise specified.

3.1.2 Lentiviral transduction of HNSCC cells

FaDu and Cal27 cells overexpressing or silenced for miR-9 expression were generated by lentiviral system as previously described [46]. Lentiviruses expressing anti-miR-9-5p (MISSION® Lenti miRNA inhibitor human has-miR-9-5p, HLTUD0946) or expressing miR-9-5p (MISSION® Lentiviral miRNA transduction particles human has-miR-9-5p, HLMIR0946) were purchased by Sigma. Cells were transduced with anti-miR-9, miR-9 control lentivirus according to the manufacturer protocol and selected in 1.0 μg/ml puromycin.
KLF5 silenced cells were generated by lentiviral system. Briefly, 293FT cells were transfected with Gag-Pol and VSV-G (Invitrogen Lentivirus Production System) plus plasmid encoding the shRNA sequence against KLF5 (sh#1 TRCN0000280277, sh#2 TRCN0000013636, sh#3 TRCN0000280340, sh#4 TRCN0000013633, sh#5 TRCN0000013637 Sigma) using calcium phosphate transfection kit (Promega), following manufacturer's protocol. After 48 and 72 h, conditional medium containing lentiviral particles was harvested and used to transduce target cells.

FuGENE HD (Promega) transfection system was used following the manufacturer's instructions to overexpress different genes in HNSCC cells. Vectors used were as follows: RSV-SP1 (Addgene #12098), pcDNA3-HA-KLF5 (Addgene #40904), pcDNA3.2/V5 miR-9 (Addgene #26317), or control vector (pEGFP-C1 or pcDNA3.1, Clontech). The p53WT and p53R273H mutant were subcloned in the pEGFP-C1 vector from the pCMV/Neo-p53R273H (Addgene#16439) into the BamHI restriction site.

Transfected cells were selected in complete medium supplemented with 500 μg/ml G418.

3.1.3 Cell viability and IC50 drug calculation

For growth curve analyses, HNSCC cells were seeded into 96-well culture plates (1 2 × 103 cells/well), and after 24h, cell proliferation was measured with CellTiter 96 AQueous cell proliferation assay kit (Promega) every day for six consecutive days.

For kill curve analyses, HNSCC cells were seeded into 96-well culture plates (2–4 × 103 cells/well), and after 24h, cells were treated with increasing doses of drugs for 72h [46] Cell viability was determined at the end of treatment using the CellTiter 96 AQueous Cell Proliferation Assay Kit (Promega).

Bleomycin (BLEO), Cisplatin (CDDP), paclitaxel (TAX), and 5-fluorouracil (5-FU) were purchased from TEVA Italia, and Cetuximab—Erbitux® was purchased from Merck.

3.1.4 Sphere-forming assay

To establish primary spheres, cells were plated (8 × 103) on poly-HEMA-coated dishes as single cell suspension in standard sphere medium containing phenol red-free DMEM/F12 (GIBCO), B27 supplement (50×, no vitamin A; Life Technologies) and recombinant epidermal growth factor (hEGF, 20ng/ml; SIGMA).After 8–10 days, primary spheres were counted and sphere area was measured with Volocity® software (PerkinElmer). To establish secondary spheres, primary spheres were collected, disaggregated in trypsin using 25-gauge needle fitted to a syringe. Cells were plated at the same seeding density of the primary generation. Sphere-forming efficiency (SFE%) was calculated using the following formula:

$$\textbf{\textit{SFE\%}} = \textit{N°. of spheres per well/N°. of cells seeded per well * 100.}$$

Sphere self-renewal was calculated as the ratio between the total number of secondary spheres divided for the total number of primary spheres.

3.1.5 Luciferase assay

Luciferase assay was performed to validate miR-9 putative target sites on KLF5 3'UTR and KLF5 putative binding site on SP1 promoter region as described [46,124]. Briefly, the sequence surrounding putative miR-9-binding sites was amplified from FaDu cell genomic DNA using specific primers. PCR products were cloned in the pGL3-control vector (Promega) digested with XbaI (Promega), at the 3' of the luciferase gene, which is under the regulation of SV40 promoter. To generate mutant KLF5 3' UTR (mutant A and mutant B), side-directed mutagenesis of the WT (wild type) KLF5 3'UTR was performed using QuickChange II Site-Directed Mutagenesis Kit (Agilent #200523) according to the manufacturer's protocol.

Progressive deletion constructs of SP1 promoter were amplified from FaDu cell genomic DNA using specific primers . PCR products were cloned unidirectionally between the NheI and XhoI sites of the reporter luciferase pGL3 basic vector (Promega). These PCR fragments were generated using a common reverse primer and five different forward primers. The numbers indicated in the primer name correspond to the distance in nt from SP1 ATG.

Luciferase assay to test miR-9 expression was performed using pMIR9 reporter vector (Addgene #25037) [125].

Briefly, CAL27, FaDu, UMSCC74B and SCC9 cells were co-transfected with 500ng of reporter constructs and 50ng of pRL-TK vector (internal control) in 24-well plate using FuGENE® HD Transfection Reagent (Promega) according to manufacturer's recommendations. After transfection cell lysates were assayed for luciferase activity using the dual-luciferase reporter assay system (Promega). Values were normalized using Renilla luciferase.

The sequences of the primers used to clone the different regions of the KLF5 3' UTR and SP1 promoter are reported below:

Primer	***Sequence 5'-3'***	***GeneBank Accession***
3'UTR KLF5 A For	TGGGCTCCCTCAAATGACAG	NM_001730
3'UTR KLF5 A Rev	ACCCCTTACCCATGTTGAGAC	NM_001730
3'UTR KLF5 B For	AGATGTTCGCTCGTGCAGTA	NM_001730
3'UTR KLF5 B Rev	GACCCCTTTTGGCATTTTGC	NM_001730
3'UTR KLF5 mut A	GGGAATACATTGTATTAATACCGGAGTGTTTG GTCATTTTAA	NM_001730
3'UTR KLF5 mut B	GCTTATTTATTCTGCCCTCCGGTTAACAGCATC	NM_001730

	AGCATCAC	
SP1 promoter -146 For	gctagcGGGCTTGTGGCGCGCTGCTC	NM_138473
SP1 promoter -281 For	gctagcGCAACTTAGTCTCACACGCCTTGG	NM_138473
SP1 promoter -443 For	gctagcCTATCAAAGCTTTGCCTATCC	NM_138473
SP1 promoter -1612 For	gctagcGGCACCTAACACGGTAGGCAG	NM_138473
SP1 promoter -20 Rev	ctcgagGCTCAAGGGGGTCCTGTCCGG	NM_138473

3.1.6 Clonogenic Assay

Cells were seeded into 6-well plates (500–2,000 cells/well depending on the cell lines) in complete medium and maintained at 37°C and 5% CO2 for 10–15 days, refreshing the medium every 3–4 days. Colonies were then fixed and stained with 0.5 mg/ml crystal violet in 20% methanol. Colonies with more than approximately 50 cells were counted manually.

3.1.7 Irradiation and survival fraction assay

Irradiations were performed using Clinac 600 C (Varian Medical Systems, Palo Alto, CA) linear accelerator (LINAC) for external beam radiation therapy, at ambient oxygen concentrations and in cell adhesion conditions. Cell plates were positioned at the center of the radiation field of 40 × 40 cm2 size, with LINAC gantry at 180°, between two 5 cm layers of solid water. The dose delivered to the cell plates was 2 or 5 Gy at a dose rate of ~ 2.5 Gy/min, as calculated from measurements with radiochromic films in the same setup of irradiation.

Given the strong effect of miR-9 in mediate an increased cell survival, we plated shCTR or miR-9/anti-miR-9 cells accordingly to obtain a similar number of colonies in the untreated condition.

The formula used to calculate the correct number of cells to be plates is the following:

N°. of cell *= N°. of optimal counting colonies/plating efficiency in standard conditions/likelihood of predicted survival.*

The survival fraction is calculated as follow:

Survival fraction*=N°. of clones in the IR condition/N°. of clones in untreated condition.*

Cells were seeded into 6-well plates or 60-mm dishes (two dilutions, in triplicate) and let adhere to the plates. Cells were then irradiated and maintained at 37°C and 5% CO2 for 10–15 days, refreshing the medium every 3–4 days. Colonies were then fixed, stained, and counted as described in the

Clonogenic Assay section. The survival fraction was expressed as the relative plating efficiencies of the irradiated cells to the control cells.

3.1.8 Anchorage-independent soft agar assay

To evaluate the anchorage-independent cell growth, 1.5×10^4 FaDu cells stably transduced with control or anti-miR-9 were resuspended in 2 ml top agar medium (DMEM + 10% FBS, 0.4% low melting agarose, SIGMA) and quickly overlaid on a previously gelified 0.6% bottom agar medium (DMEM + 10% FBS, 0.6% low melting agarose, SIGMA). The experiments were performed in six-well tissue culture plates, in triplicate. Fresh medium was added to the wells twice a week as a feeder layer. After three weeks, the number of colonies was counted in 10 randomly chosen fields, at 10× magnification.

3.2 Molecular biology experiments

3.2.1 RNA extraction and qRT–PCR analyses

Total RNA for qRT–PCR analyses was isolated from HNSCC primary tumors or cell cultures using TRIzol solution (Roche Applied Science Mannheim, Germany) according to manufacturer protocol. GentleMACS™ Dissociator (Miltenyi Biotec) was used to disrupt HNSCC primary tumors, and lysates were passed at least five times through a 23-gauge needle fitted to an RNase-free syringe. Total RNA was quantified using NanoDrop (Thermo Fisher Scientific Inc., USA).

The expression of miR-9-5p was analyzed using the TaqMan single-tube MicroRNA Assays (#000583 Thermo Fisher Scientific). All reagents, primers, and probes were obtained from Applied Biosystems. Reverse Transcriptase (RT) reactions and qRT–PCR were performed according to the manufacturer instructions (Applied Biosystems, Life Technologies). Normalization was performed on the U6 RNA (#001973 Thermo Fisher Scientific). All RT reactions were run in an T100 Thermal Cycler (Bio-Rad). Comparative qRT–PCR was performed in triplicate, including no-template controls. miR levels were quantified using the CFX384 (Bio-Rad). Relative expression was calculated using the comparative Ct method.

For gene expression analysis, RNA was retro-transcribed with GoScript Reverse Transcriptase to obtain cDNAs, according to provider's instruction (Promega). Absolute quantification of targets was evaluated by qRT–PCR, using SYBR Green dye-containing reaction buffer (SsoFast Master Mix 2×, Bio-Rad). The incorporation of the SYBR Green dye into the PCR products was monitored in real-time PCR, using the CFX384 Real-time PCR Detection System (Bio-Rad). Ct values were converted

into attomoles, and normalized expression was evaluated by using SDHA and actin as housekeeping genes. Primers used in qRT–PCR are reported as follow:

Gene	***Primer Forward 5' – 3'***	***Primer Reverse 5' – 3'***	***GeneBank ID***
SP1	GGTGCCTTTTCACAGGCTC	CATTGGGTGACTCAATTCTGCT	NM_138473
KLF5	CCCTTGCACATACACAATGC	AGTTAACTGGCAGGGTGGTG	NM_001730
GAPDH	GAAGGTGAAGGTCGGAGTC	GAAGATGGTGATGGGATTTC	NM_001289746.1

3.2.2 Droplet Digital PCR (ddPCR) assay

Total RNA for ddPCR analyses was isolated from FFPE HNSCC biopsies as described above. Total RNA was retro-transcribed and converted in cDNA using TaqMan-based technology. Briefly, this technology incorporates a target-specific stem-loop reverse-transcription primer which extends the length of mature microRNA (~ 22 bp) at its 3'. The resulting chimera, consisting of mature microRNA and the stem-loop primer, represents a template of a sufficient length to be analyzed with standard real time or ddPCR using TaqMan assays. Following cDNA synthesis, ddPCRs were prepared in a similar manner as qRT–PCRs. Briefly, ddPCR is composed by 1 ng RNA-equivalent cDNA, ddPCR™ supermix for probes (no dUTPs 2x—Bio-Rad) and the properly TaqMan probes for analyzing miR-9 and U6 (Applied Biosystems). The droplet generations were performed in a QX200 Droplet Generator (Bio-Rad) using Droplet Generation Oil for Probes (Bio-Rad) according to the manufacturer protocol. Thermocycling of the microfluidic emulsions was achieved in an Epp twin tec PCR plate 96 semi-skirted (Eppendorf) using T100 Thermocycler (Bio-Rad). PCR thermocycling was initiated with a 10 min "hot start" at 95°C to activate the polymerase, followed by 40 cycles at 94°C for 30 s and 59°C for 30 s, and the last step to inactivate the enzyme at 98°C 10 min. miR-9 and U6 absolute quantification were achieved using QX200 Droplet Reader (Bio-Rad), and data were analyzed with QuantaSoft (Bio-Rad).

3.2.3 Protein extraction, immunoprecipitation, and western blot analysis

For cellular protein lysates, cells were scraped on ice using cold Ripa lysis buffer (150 nM NaCl, 50 mM Tris–HCl pH 8, 1% Igepal, 0.5% sodium deoxycholate, 0.1% SDS) supplemented with a protease inhibitor cocktail (CompleteTM, Roche), 1 mM Na3VO4 (Sigma), 100 mM NaF (Sigma), and 1 mM

DTT (Sigma). Proteins were separated in 4–20% SDS–PAGE (Criterion Precast Gel, Bio-Rad) and transferred to nitrocellulose membranes (GE Healthcare).

Immunoprecipitations were performed using cell lysates in HNTG buffer (20 mM Hepes, 150 mM NaCl, 10% glycerol, and 0.1% Triton X-100) and the indicated primary antibody [anti–KLF5 (no. 11814460001, Roche), anti-P53DO1 (anta Cruz Biotechnology), and incubated overnight at 4°C. The immunocomplexes were precipitated by adding protein G agarose conjugated for an additional 1 hour and 30 min at 4°C. IPs were then washed in HNTG buffer, resuspended in 3× Laemmli Sample Buffer [5× Laemmli buffer composition: 50 mM tris-HCl (pH 6.8), 2% SDS, 10% glycerol, 0.05% bromophenol blue, and 125 mM β-mercaptoethanol], and finally separated on SDS-PAGE for Western blot analysis. Membranes were blocked with 5% dried milk in TBS-0,1% Tween 20 or in Odyssey Blocking Buffer (LI-COR, Biosciences) and incubated at 4°C overnight with primary antibodies. The list of primary antibodies is provided in Table 1.

Membranes were washed in TBS-0,1% Tween 20 and incubated 1h at RT with IR-conjugated (AlexaFluor680, Invitrogen or IRDye 800, Rockland) secondary antibodies for infrared detection (Odyssey Infrared Detection System, LI-COR) or with the appropriate horseradish peroxidase-conjugated secondary antibodies (GE Healthcare) for ECL detection (Clarity Western ECL Substrate, Bio-Rad). Band quantification was performed using the Odyssey v1.2 software (LI-COR) or the QuantiONE software (Bio-Rad Laboratories). The Re-Blot Plus Strong Solution (Millipore) was used to strip the membranes, when reblotting was needed.

Primary Antibodies	***Catalog Number***	***Vendor***	***Application and Dilution***
SASH1	#A302-265A	Bethyl	WB (1:500)
GAPDH	6C5	Calbiochem	WB (1:1000)
pY1068-EGFR	#3777	Cell Signaling	WB (1:1000)
β-Actin	#8457	Cell Signaling	WB (1:2000)
pT202-Y204-ERK1/2	#9101	Cell Signaling	WB (1:1000)
ZO-1	#8193	Cell Signaling	WB (1:500)
Histone H3	#4499	Cell Signaling	WB (1:1000)
KRT13	#SAB2104755	Millipore-Sigma	WB (1:500)
α-Tubulin	#T8203	Millipore-Sigma	WB (1:2000)
SP1	#SAB140397	Millipore-Sigma	WB (1:500)
P53-DO1	#OP43L	Millipore-Sigma	WB (1:1000)
pS139-H2AX (γH2AX)	#05-636	Millipore-Sigma	WB (1:1000), IF (1:500)
pS10-H3	#06-570	Millipore-Sigma	WB (1:1000), IF (1:500)

KLF5	sc-398470	Santa Cruz	WB (1:500)
ERK1/2	sc-271269	Santa Cruz	WB (1:1000)
EGFR	sc-03	Santa Cruz	WB (1:1000)
Vinculin	sc-73614	Santa Cruz	WB (1:1000)
Ki67 clone 30-9	#70-4286	Ventana	IHC (1:500)

Table 1: Primary Antibodies. *The table summarizes the primary antibodies (catalog number and vendor) and the dilution used in the different experiments. WB: Western Blot, IF: Immunofluorescence, IHC: Immunohistochemistry.*

3.2.4 Chromatin immunoprecipitation assay

FaDu and CAL27 cells were treated with 1% formalehyde, and chromatin was prepared via MNase enzymatic digestion according to the protocol. Chromatin immunoprecipitation (IP) was performed using SimpleChIP Enzymatic Chromatin IP kit—Magnetic Beads (#9003, Cell Signaling Technology). After IPs, DNA was purified and analyzed by qRT–PCR. Signals obtained from each IP are expressed as % of the total input chromatin. PCRs included the positive control histone H3, and the negative control Normal Rabbit IgG. The 2% of the amount of the chromatin is used for the input; thus, a 50-fold dilution factor has been taken into account (Log2(50) = 5.64 cycles), to calculate the adjusted input Ct value (100%), as follows:

$$\textbf{\textit{Adjusted Input Ct}} = Ct[Input] - [Log2(50)]$$

Then calculation of ΔCt was obtained, following the formula:

$$\textbf{\textit{}}\Delta Ct = Ct\ (Adjusted\ Input) - Ct\ (sample\ of\ interest)$$

Finally, % of Input was obtained for each sample: ***% of Input*** = 100 * 2(ΔCt) representing the enrichment of antibody binding onto specific regions of SP1 promoter. The primers used to amplify the indicated SP1 promoter regions and positive and negative controls of the anti-KLF5 antibody derived from the literature are reported following:

Amplified Region	***Primer Forward 5' – 3'***	***Primer Reverse 5' – 3'***
SP1 -253/+7	GCAAGCGAGTCTTGCCATTGG	CGCTCATGGTGGCAGCTGAGG
SP1 -480/-230	ATATCCCGGATTCTGGTTGGC	ATCCAATGGCAAGACTCGCT
SP1 -673/-486	GCCCTCAGTTAATTCGGCGT	GCAAAATCCTAGTGGGCGGA
SP1 -891/-674	CGCTAAAGCGTCCCACCTAA	GAAACTTGGAGTGGCAGAGGA
SP1-1602/-1402	CGGTAGGCAGTCAGCAATCA	CCGGCCTTAATAGCTTGTCA

3.2.5 Immunofluorescence analysis

For immunofluorescence analyses on cultured cells, cells were seeded in wells containing round coverslips (Thermo Fisher Scientific) and then, at specified time points, fixed 10 min in 4% PFA, permeabilized 5 min in PBS 0.2% Triton, and blocked 1h in PBS-5% normal goat serum (NGS). Incubation with primary antibodies (pS10-H3 #06-570 and pS139-H2AX (γH2AX) #05-636 Millipore) was performed ON at 4°C. Incubations with primary antibodies were followed by 1h at RT with secondary antibody (Alexa Fluor 633, 568 or 488, Invitrogen). Propidium iodide (3 μg/ml) containing RNaseA (100 μg/ml) or TO-PRO in PBS 1× was used to stain nuclei (respectively, 20 and 5 min at RT) and Alexa 546-conjugated phalloidin (Molecular Probes) for the actin staining (1h at RT). Stained cells were observed using a confocal laser-scanning microscope (TSP2 or TSP8 Leica).

3.2.6 Histological analysis and immunohistochemistry

Mouse xenograft samples were fixed in formalin (overnight at 4°C) and processed for standard paraffin embedding. Histological sections (5 μm thick) were made from the paraffin blocks, deparaffinated with xylene, and stained with hematoxylin and eosin (H&E), according to standard procedures. Images were collected with Leica microscope to measure the percentage of necrotic area in tumor section. Routine deparaffinization of all sections mounted on positive charge slides was carried out according to standard procedures, followed by rehydration through serial ethanol treatments. Slides were immersed in citrate buffer [0.01 M sodium citrate (pH 6.0)] and heated in a microwave oven at 600W for 3 times, 5 min each, to enhance antigen retrieval. Endogenous peroxidase was blocked with 0.3% hydrogen peroxide in methanol for 30 min. Sections were immunostained with Ki67 antibody (Table 1) according to manufacturer's protocol and standardized procedures.

3.2.7 TUNEL assay

Detection of apoptosis was performed with TUNEL assay, using In Situ Cell Death Detection Kit, AP (Roche) on sections from FFPE HNSCC xenografts, according to the manufacturer's instructions. Apoptosis was calculated as the ratio of positive cells over the total number of cells per field. At least four different mice for each group and 10 fields/slice were analyzed.

3.3 Animal studies

Animal experimentation was approved our Institutional Animal Care and Use Committee (OPBA) and conducted strictly complying with internationally accepted guidelines (IACUC) for animal research and following the 3Rs' principles.

To evaluate the tumor growth and onset of HNSCC cells, primary tumors were established by subcutaneous injection of 1×10^6 FaDu (4 mice) or 5×10^6 CAL27 (3 mice) parental cells bilaterally in the flanks of female athymic nude mice (Charles River, 6 weeks old). Growth of primary tumors was monitored by measuring tumor width (W) and length (L) with a caliper three times per week and calculating tumor volume based on the formula: Tumor volume (mm3) = (W2 × L)/2.

To evaluate the role of miR-9 in tumor growth and onset, primary tumors were established by subcutaneous injection of $0.5–2 \times 10^6$ FaDu (control and anti-miR-9) or CAL27 (control or miR-9) cells bilaterally in the flanks of female NSG mice or by subcutaneous injection of 1×10^6 CAL27 (control and anti-miR-9) cells, bilaterally in the flanks of female NSG mice (Charles River, 6 weeks old). Growth of primary tumors was monitored as described above.

To evaluate the role of miR-9 in response to radiotherapy and/or Cetuximab primary tumors were established by subcutaneous injection of 1.5×10^6 FaDu parental cells (Day 0) bilaterally in the flanks of female athymic nude mice (Charles River, 6 weeks old). Growth of primary tumors was monitored as described above.

At days 6, 9, and 15 after cell injection, when tumors reached a volume of 15–20 mm^3, pre-anesthetized mice received an intra-tumor injection of high-titer lentiviral particles (control or anti-miR-9-5p, MISSION® Lenti miRNA inhibitor transduction particles, SIGMA). Mice were randomly divided into four groups according to experimental design (5 mice/group). Pre-anesthetized mice were subjected to radiotherapy 4 Gy/tumor at days 13, 20, 27, and 34 after injection. Radiotherapy was administered using Clinac 600 C (Varian Medical Systems, Palo Alto, CA) linear accelerator (LINAC) for external beam radiation therapy at 2 Gy/min dose. Vehicle or Cetuximab (8 mg/kg) was administered intraperitoneally two days before, the same day, and two days after radiotherapy. Unless tumor burden was incompatible with the well-being of the animals, mice were sacrificed at the end of the experiment and pathologically examined.

3.4 Patient samples and study approval

Specimens from primary HNSCC (Table 2) were collected from patients who underwent surgery at our Institutie and at Santa Maria degli Angeli Hospital, Pordenone, Italy. HNSCC specimens were immediately frozen and stored at −80°C. Paraffin-embedded samples of radiotherapy plus

Cetuximab-treated HNSCC patients were obtained from the Santa Maria degli Angeli Hospital Pordenone, Italy, from Isontina Hospitals (Monfalcone and Gorizia, Italy) and from the Fondazione Policlinico Universitario Agostino Gemelli, Università Cattolica del Sacro Cuore, Rome, Italy. The study was approved by the Internal Review Board of the Centro di Riferimento Oncologico (CRO) of Aviano (#IRB-08/2013). A written informed consent was obtained from all patients included in this study, and the experiments conformed to the principles set out in the WMA Declaration of Helsinki and the Department of Health and Human Services Belmont Report.

For the analysis of miRNA-9 expression levels in the TCGA dataset, we retrieved the information from 31 HNSCC tissue samples collected from patients treated with Cetuximab and radiotherapy (cohort 1). The Kaplan–Meier method was performed to generate survival curves and the statistical significance of the difference between survival curves of high- vs. low-expression groups was evaluated using the log-rank test. The cut-off point for the two groups was changed iteratively (P-values less than 0.01 were considered to be significant), and the cut-off that obtained the most significant P value was selected.

Head and Neck Cancer Samples	
Characteristic	**Value**
Age - Year	
Median	64
Range	33 -92
Cancer site - no. (%)	
Oral cavity / Tongue	58 (38.7)
Tongue	5 (3.3)
Oro-Pharynx	46 (30.7)
Hypo-Pharynx	11 (7.3)
Larynx	26 (17.3)
Tonsil	3 (2)
Nasal Cavity	1 (0.7)
Tumor Grade - no. (%)	
G1	10 (6.7)
G2	78 (52.0)
G3	53 (35.3)
Not Available or Specified	9 (6.0)
Histology - no. (%)	
SCC*	150 (100)
cT** - no. (%)	
T1	33 (22)
T2	56 (37.3)
T3	27 (18)
T4	29 (19.4)
Not Available or Specified	5 (3.3)
cN*** - no. (%)	
N0	73 (48.67)
N1	28 (18.67)
N2	37 (24.67)
N3	2 (1.33)
Not Available or Specified	10 (6.67)

Table 2: Features of the patients from whom HNSCC samples were collected, at Centro di Riferimento Oncologico (CRO) of Aviano. *The table summarizes the pathological and histological tumor status in HNSCC cohort collected at the CRO of Aviano. * SCC = Squamous Cells Carcinoma; ** cT = Clinical Tumor size*** cN = Clinical Node Status.*

3.5 Statistical analyses

For the *in vivo* studies, no statistical methods were used to predetermine sample size. The experiments were not randomized, but mice were assigned to the different groups according to their age and then randomly assigned to treatment arms.

Tumor volumes were measured by the non-blinded investigator with the caliper, and no subjective methods were applied. Animals were randomized to the different treatment groups (i.e., vehicle, radiation, Cetuximab, or the combination), and no exclusion criteria were applied.

All graphs and statistical analyses were performed using PRISM (version 6, GraphPad, Inc.) and R, SAS Software 9.2. In all experiments, differences were considered significant when P was < 0.05. Statistical analyses including Kaplan–Meyer survival analyses, paired and unpaired t-tests, Mann–Whitney unpaired t-test and Spearman correlation test, one-way and two-way ANOVA test, and Sidak's multiple comparison test were used as appropriate and as specified in each figure.

4. RESULTS

4.1 miR-9 regulates the plasticity of HNSCC-derived cells

Based on literature data, indicating that miR-9 regulates cell plasticity and cancer stem cell-like phenotypes in SCC [48] and from data from our lab, demonstrating that its expression is strongly associated with recurrence risk in HNSCC patients [46], we decided to investigate further the role of miR-9 in HNSCC onset and progression.

miR-9 is expressed at different levels among the HNSCC-derived cell lines. FaDu and SCC9 cells lines displayed the highest, while CAL27 and UMSCC1 cell lines displayed the lowest miR-9 expression, comparable with the one of normal epithelial cells (NHBE) (Fig. 1A). *In vivo*, FaDu cells (miR-9 high) grew much faster than CAL27 cells (miR-9 low), even when a lower number of cells was injected (1×10^6 FaDu *vs* 5×10^6 CAL27) (Fig. 1B). These cell lines have then been used to characterize the role of miR-9 in HNSCC cell growth and response to therapies.

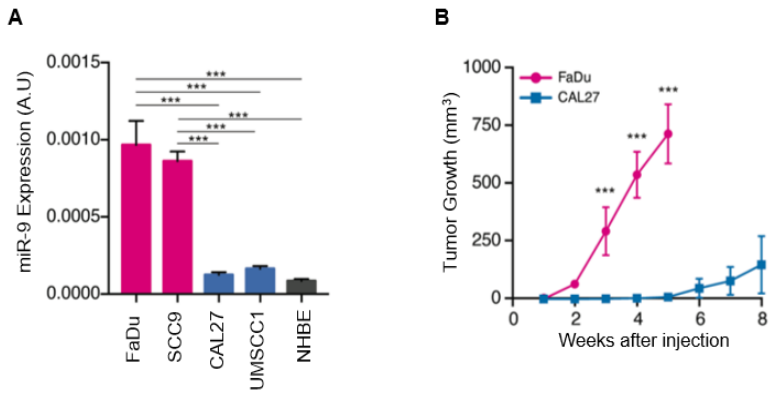

Fig. 1: miR-9 is differently expressed among the HNSCC-derived cell lines and its expression is associated with higher in vivo growth of HNSCC cells. A) *qRT-PCR analyses of normalized miR-9 expression in FaDu, SCC9, CAL27 and UMSCC1 cancer cells and NHBE normal epithelial cells. Data are the mean (±SD) of three independent experiments performed in duplicate. A.U. = Arbitrary Units.* ***B)*** *Graph reports the mean value (±SD) of tumor volume in nude mice injected in both flanks with $1x10^6$ FaDu (n=4 mice) or $5x10^6$ CAL27 cells (n=3 mice) followed for up to 8 weeks. ***P < 0.001.*

To this aim, we first generated stable FaDu cells expressing the anti-miR-9 or an empty vector (shCTR) (Fig. 2A). Anti-miR-9 FaDu cells showed an increased expression of SASH1 and KRT13, already identified as miR-9 targets in HNSCC cells [46], and of the epithelial marker ZO-1, compared to control FaDu cells (Fig. 2B). These differences were accompanied by a strong decrease in the ability to grow both in anchorage-dependent and in anchorage-independent manner, as demonstrated by growth curves, clonogenic and soft agar assays, respectively (Fig. 2C–E). Anti-miR-9 FaDu cells displayed lower sphere-forming and self-renewal abilities, in terms of both number and size of the spheres (Fig. 2F). Moreover, in line with these *in vitro* data, upon transplantation in animals, antimiR-9 FaDu cells formed smaller tumors with a longer latency, compared to shCTR cells (Fig. 2G-H).

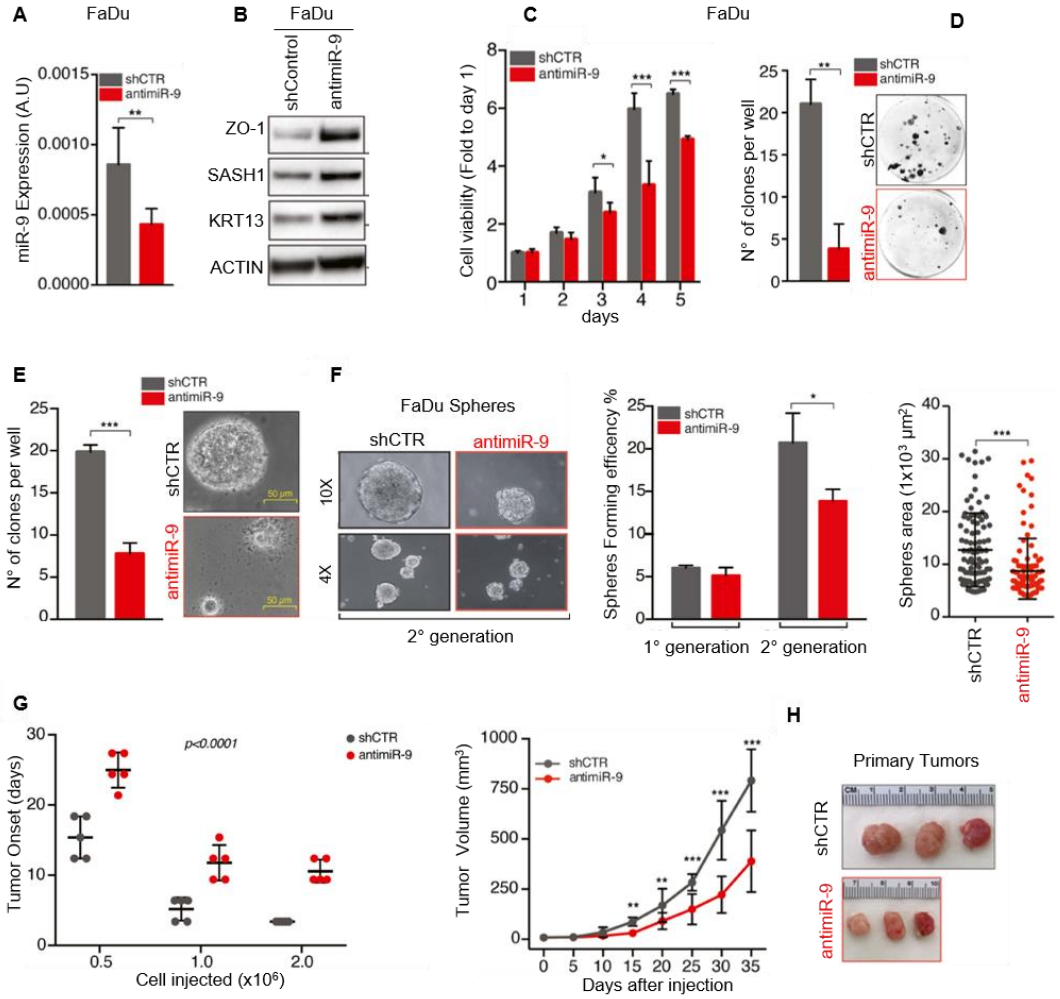

Fig. 2: miR-9 increases the tumor-initiating properties in HNSCC-derived cells*. **A)** qRT–PCR analyses of miR-9 expression in control (shCTR) and anti-miR-9 FaDu cells. Data represent the mean (± SD) of three independent experiments performed in duplicate. **B)** Western blot (WB) analyses of the indicated protein expression in shCTR and antimiR-9 FaDu.cells Actin was used as loading control. **C)** Cell viability analyses of FaDu cells over a period of 5 days using the MTS assay. Data represent the mean (± SD) of three independent experiments performed in sextuplicate. **D)** Colony formation assay of the FaDu cells. Left graph reports the number of clones per well. Data represent the mean (± SD) of three independent experiments performed in duplicate. Right, representative images of clones are shown. **E)** Soft agar assay of the FaDu cells. Left graph reports the number of clones per well. Data represent the mean (± SD) of three independent experiments performed in duplicate. Right, representative images of 10X field are shown. **F)** Sphere-forming assay of the cells. Left images of 4X and 10X fields are shown. Middle graph reports the number of spheres formed in first and second generations. Right graph reports the area of second-generation spheres. Each dot represents one analyzed sphere. Data represent the mean (± SD) of three independent experiments performed in duplicate. In A-C-D-E-F) unpaired t-test was used for the statistical analysis. **G)** Graph reporting the tumor onset in NSG mice injected with control (shCTR) and antimiR-9 FaDu cells, and followed for up to 35 days (n = 5 mice/group). Data represent the mean (± SD), and two-way ANOVA test was used to calculate the statistical significance among groups. **H)** Graph reports the tumor volume in NSG mice injected with control (shCTR) and antimiR-9 FaDu cells followed for up to 35 days (n= 5 mice/group). Data represent the mean (± SD), and unpaired t-test was used to verify the statistical significance at each time point. On the right, typical images of explanted tumors formed by control (shCTR) and antimiR-9 FaDu cells at necropsy. *P < 0.05; **P < 0.01; ***P < 0.001.*

We also assessed the opposite approach and stably overexpressed miR-9 in CAL27 cells, and observed that miR-9 overexpression led to decreased expression levels of SASH1, KRT13, and ZO-1, associated with increased proliferation potential, with higher colony- and sphere-formation capabilities (Fig. 3A–E). Accordingly, upon transplantation in animals, miR-9 overexpressing CAL27 cells formed bigger tumors and shorter latency, compared with controls (Fig. 3F-G).

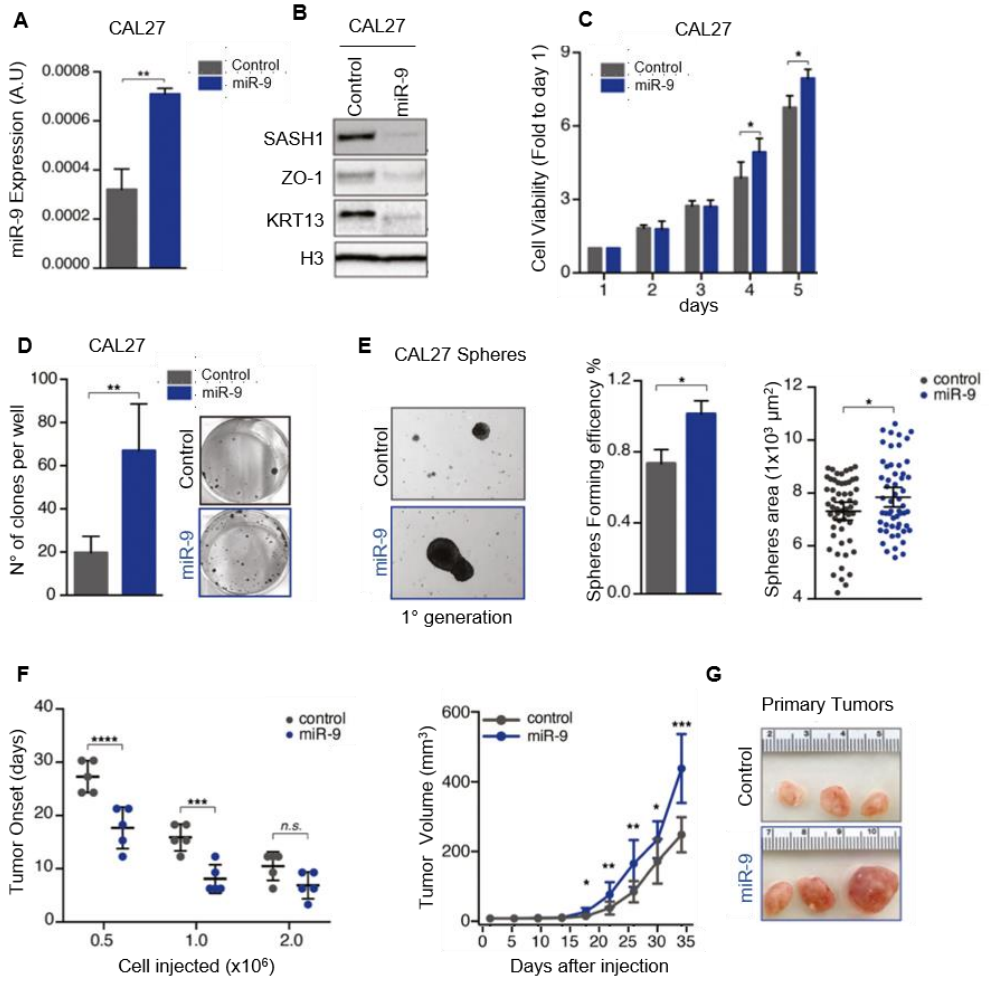

Fig. 3: miR-9 overexpression increases the tumor-initiating properties of HNSCC cells*. **A)** qRT–PCR analyses of normalized miR-9 expression in control and miR-9 overexpressing CAL27 cells. Data represent the mean (± SD) of three independent experiments performed in duplicate. **B)** Western blot analyses of the indicated protein expression in CAL27 cells described in (A). Histone H3 was used as loading control. **C)** Cell viability analyses of CAL27 cells over a period of 5 days using MTS cell viability assay. Data represent the mean (± SD) of three independent experiments performed in sextuplicate. **D)** Colony formation assay of cells described in (A, B). Left graph reports the number of clones per well. Right, representative images of clones are shown. Data represent the mean (± SD) of three independent experiments performed in duplicate. **E)** Sphere-forming assay of cells described in (A, B). On the left, typical images of 10X field are shown. Middle graph reports the sphere-forming efficiency and in the right, graph reports the area of first-generation spheres. Each dot represents one analyzed sphere. Data represent the median (± SD) of three independent experiments performed in duplicate. In A-C-D-E), unpaired t-test was used for the statistical analysis. **F)** Graph reports the tumor volume (mean ± SD) in NSG mice injected with control and miR-9 overexpressing CAL27 cells followed for up to 35 days (n = 5 mice/group). Data represent the mean (± SD), and two-way ANOVA test was used to calculate the statistical significance among group. **G)** Graph reporting the tumor onset (mean ± SD) in NSG mice injected with shCTR and miR-9 overexpressing CAL27 cells and followed for up to 35 days (n = 5 mice/group). Unpaired t-test was used to verify the statistical significance at each time point. On the right, typical images of explanted tumors formed by control and miR-9 CAL27 cells at necropsy. *P < 0.05; **P < 0.01; ***P < 0.001.*

4.2 miR-9 expression is positively regulated by EGFR activation

Our data suggested that miR-9 expression was able to strongly regulate HNSCC plasticity and tumor initiating features. Thus, we asked how this miRNA was regulated in HNSCC cells. Several evidences in literature indicated that miR-9 expression correlates with cell proliferation and is positively

regulated by the activation of RAS and c-Myc in breast cancer [125], suggesting that mitogenic stimuli may positively regulate miR-9 transcription also in HNSCC. In accord with this hypothesis, a luciferase assay demonstrated that serum stimulation increased by threefold the promoter activity of miR-9, starting at 1h from serum addition (Fig. 4A).

EGFR is one of the most frequently amplified/mutated growth factor receptors in primary HNSCC and its critical biological role in many cancer types has represented the rationale for the development of targeted anti-EGFR treatments. We thus tested whether EGFR activation could regulate miR-9 expression. Our experiments showed that EGF stimulation increased by threefold the expression of endogenous miR-9 (Fig. 4B). On the contrary, inhibition of EGFR with Cetuximab (CTX), a monoclonal antibody approved for the treatment of HNSCC patients in combination with RT, decreased the activity of miR-9 promoter reducing also the miR-9 expression, in both control and anti-miR-9 FaDu cells (Fig. 4C–D).

These data suggested that miR-9 could interfere with the response to anti-EGFR-targeted therapy and modulate its response. In accord with this hypothesis, miR-9 silencing sensitized FaDu cells to EGFR inhibition by CTX treatment (Fig. 4E); while miR-9 overexpression protected CAL27 cells from CTX-induced cell death (Fig. 4F).

As a further indication of the presence of a biological link between miR-9 and EGFR, we observed that EGFR and miR-9 expression levels significantly correlated in a cohort of primary HNSCC samples (n. 150) analyzed by qRT-PCR (Fig. 4G).

Overall, these data support that miR-9 could be implicated in the response to anti-EGFR treatments.

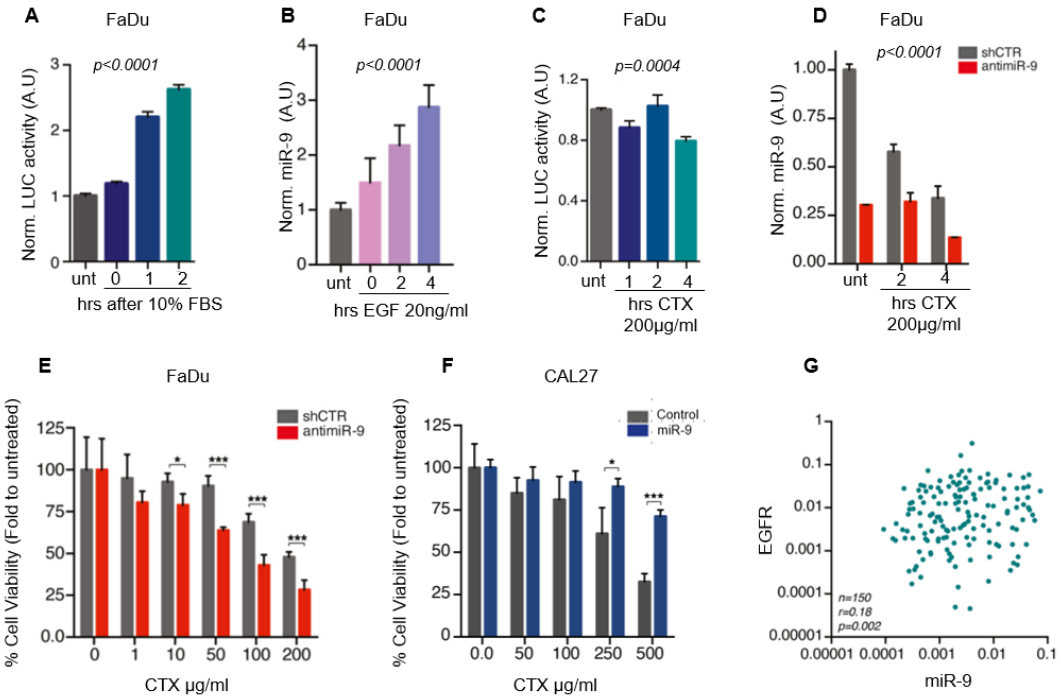

Fig. 4: miR-9 expression is induced by EGFR pathway activation in HNSCC. A) *Graph reporting the normalized luciferase activity of miR-9 promoter, expressed as fold over the untreated condition, in FaDu cells serum starved and then stimulated with 10% fetal bovine serum (FBS) for 1 and 2h.* ***B)*** *qRT–PCR analyses of normalized miR-9 expression, expressed as fold over the untreated condition, in FaDu cell serum starved and then stimulated with 20 ng/ml of epidermal growth factor (EGF) for 2 and 4h.* ***C)*** *Normalized luciferase activity of miR-9 promoter, expressed as fold over the untreated condition, in FaDu cells treated with Cetuximab (CTX) for 1-2 and 4h. In A-B-C), data represent the mean (± SD) of three independent experiments performed in duplicate, and one-way ANOVA test was used for the statistical analysis.****D)*** *qRT–PCR analyses of normalized miR-9 expression, expressed as fold over the untreated condition, in shCTR and antimiR-9 FaDu cells treated with CTX for 2 and 4h. Data represent the mean (± SD) of three independent experiments performed in duplicate, and two-way ANOVA test was used to verify the statistical significance.* ***E-F)*** *Cell viability of shCTR and antimiR-9 FaDu cells (E) and Control and CAL27 miR-9 overexpressing cells (F) treated with increasing concentration of CTX as indicated and evaluated using the MTS assay. Data represent the mean (± SD) of two independent experiments performed in sextuplicate, and unpaired t-test was used to verify the statistical significance per each dose.* ***G)*** *Dot plot reporting the correlation of EGFR and miR-9 expression in primary HNSCC samples evaluated by qRT–PCR. The number of analyzed samples (n), the Spearman correlation value (r), and its significance (P) are reported in the graph. *P < 0.05; **P < 0.01; ***P < 0.001.*

4.3 miR-9 regulates the response to radiotherapy, but not to chemotherapy, in HNSCC cells

Next, we tested whether miR-9 expression was implicated in tumor response to the standard chemo- and radio-therapy used for treatment of HNSCC patients.

To this aim, we treated FaDu and CAL27 cells with cisplatin (CDDP), 5-fluorouracil (5-FU), paclitaxel (TAX), and the radiomimetic drug bleomycin (BLEO) (purchased from TEVA, Italia), in line with what is currently used in clinics. When administered as single agents, only bleomycin was found to be more effective in FaDu antimiR-9 cells and less in miR-9 overexpressing CAL27 cells, compared to corresponding controls (Fig. 5A-B).

This result suggested a specific role for miR-9 in protecting from radiation-induced cell death. To validate this finding, we irradiated cells with 2 or 5Gy of irradiation (IR), depending on the sensitivity of each cell line, and tested the ability of miR-9 to protect cells from IR-induced death. Indeed, FaDu antimiR-9 cells, showed lower mir-9 levels post IR respect to the control and were more sensitive to IR-induced death (Fig. 5C-D), while CAL27 cells stably overexpressing miR-9 were more IR-resistant (Fig. 5F) compared to their control counterpart.

To verify whether miR-9 could affect the IR-induced DNA damage response (DDR), we assessed the expression of γH2AX (DNA damage marker) both in miR-9 silenced FaDu cells and in miR-9 overexpressing CAL27 cells, compared to corresponding controls. We irradiated cells and allowed them to repair the DNA damage for 8–24 hours. In both the cell lines, a rapid and stronger γH2AX expression was observed when miR-9 expression was lower than controls (Fig. 5E and G).

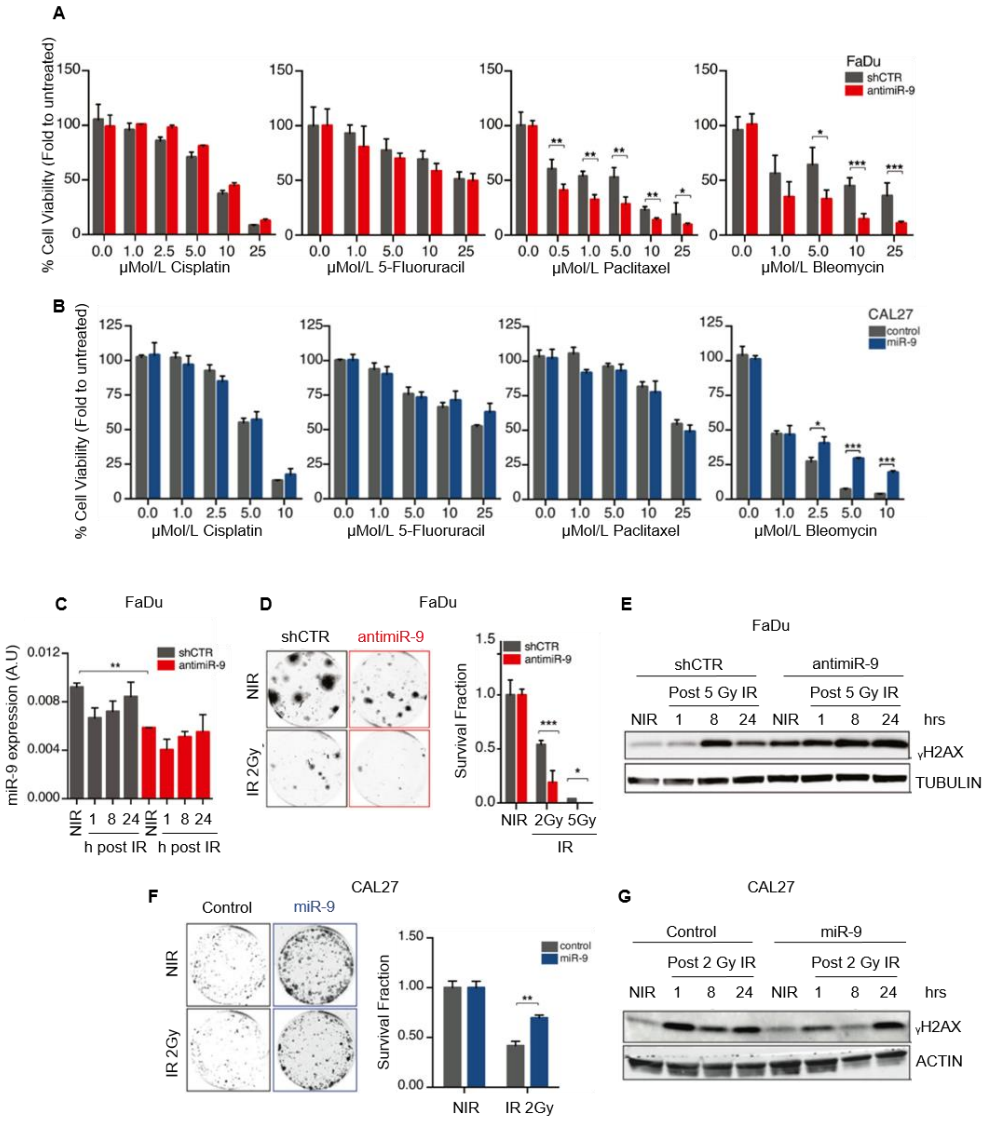

Fig. 5: miR-9 protects HNSCC cells from RT-induced cell death. A-B) *Graphs reporting cell viability of FaDu cells (shCTR and antimiR-9) and CAL27 cells (control and miR-9) treated with increasing concentration of the indicated drugs for 72h and analyzed using the MTS cell viability assay. Data represent the mean (± SD) of three independent experiments*

each performed in sextuplicate. ***C)*** *qRT–PCR analyses of miR-9 normalized expression in FaDu cells not irradiated (NIR) or treated with 5 Gy IR and allowed to repair for the indicated hours. Data are the mean (± SD) of three independent experiment performed in duplicate.* ***D-F)*** *Clonogenic assays of FaDu cells (shCTR and antimiR-9) and CAL27 cells (control and miR-9) not irradiated (NIR) or treated with 2 or 5 Gy IR. Left, typical images of cell clones are shown. On the right, the graph reports the percentage (± SD) of survived cells respect to the NIR cells in three independent experiments performed in triplicate.* ***E-G)*** *WB analyses of the indicated protein expression in FaDu cells (shCTR and antimiR-9) and CAL27 cells (control and miR-9) NIR or treated with 2 or 5 Gy IR and allowed to repair for the indicated hours (hrs). Tubulin and Actin were used as loading control in FaDu and CAL27 cells respectively. In A-B-C-D-E-F) unpaired t-test was used to calculate the statistical significance per each dose of drugs and IR. *P < 0.05; **P < 0.01; ***P < 0.001.*

These data were also confirmed by immunofluorescence analyses of γH2AX coupled with pSer10-H3 (marker of mitosis), in FaDu and CAL27 cells modified for miR-9 expression, treated as above. miR-9 silencing did not affect the M phase, but increased the number of damaged cells (γH2AX positive) and the time necessary to repair the damage (Fig. 6A), while its overexpression significantly reduced the number of γH2AX-positive cells and accelerated the recovery after the IR-induced cell cycle arrest, measured as % of pSer10-H3-positive cells (Fig. 6B).

Overall, these results support a putative impact of miR-9 in the response to DNA damage following IR.

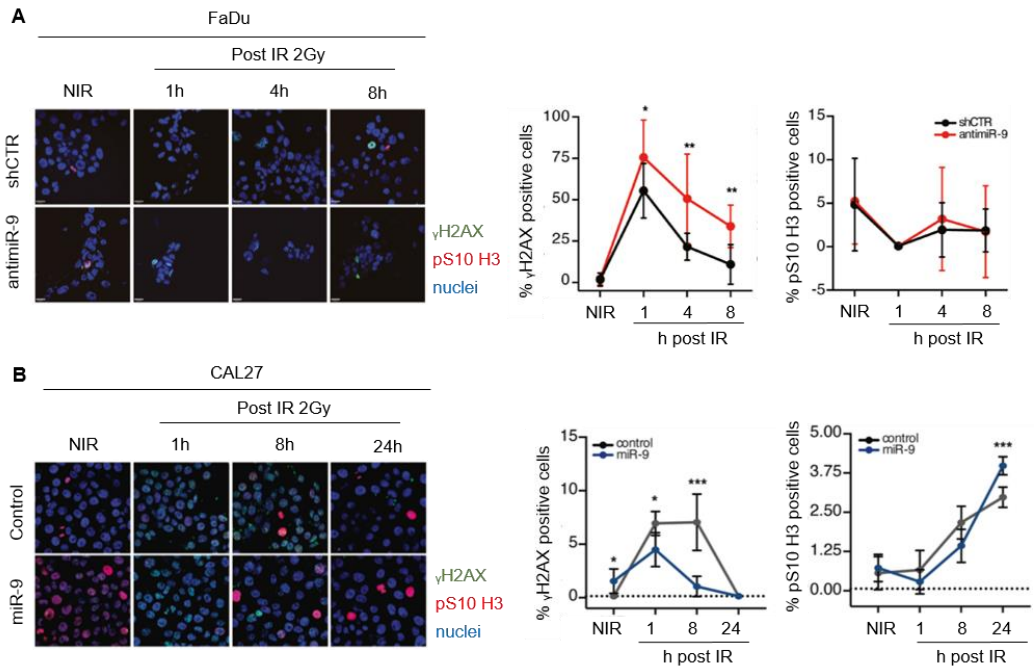

Fig. 6: miR-9 protects HNSCC cells from RT-induced cell death. A-B) *Left, typical Immunofluorescence images of FaDu shCTR and antimiR-9 cells (A) and CAL27 control and miR-9 cells (B) not irradiated (NIR) and analyzed 1, 4, or 8h (FaDu) and 1, 8, 24h (CAL27) after 2Gy IR (γH2AX green, pS10-H3 red, nuclei in blue). Right, graphs report the percentage of γH2AX and pS10-H3 positive cells. Data represent the mean (± SD) of three independent experiments in which at least 5 randomly selected fields were evaluated. Unpaired t-test was used to calculate the statistical significance at each time point.*

4.4 miR-9 regulates the response to RT+CTX, also *in vivo*

The data collected so far demonstrated that high levels of miR-9 correlated with resistance to both anti-EGFR and IR treatments in HNSCC cells. Thus, we next verified whether these data were also confirmed in *in vivo* settings.

We subcutaneously injected mice with control and antimiR-9 FaDu cells and, after tumor onset, mice were divided into two groups: one group was treated with CTX (1 mg/kg), administered two times a week, for three weeks and the other with vehicle. First, we observed that tumor appearance was significantly delayed in antimiR-9 FaDu cells; moreover, CTX was not able to reduce the *in vivo* growth of FaDu cells, either control or antimiR-9 (Fig. 7A). However, western blot analyses on tumor lysates confirmed a mild activity of CTX in reducing EGFR and ERK phosphorylation, compared to tumors treated with vehicle (Fig. 7B).

Given the fact that miR-9 silencing greatly affected tumor initiation and growth, it was difficult to further analyze miR-9 effect on tumor progression and response to therapies. To overcome this problem, we generated high-titer lentiviral particles encoding for an empty vector (shCTR) or antimiR-9 and injected them intra-tumor when masses formed by subcutaneously injected FaDu parental cells reached 15–20 mm^3 of volume. Then, as depicted in Fig. 7C, four cycles of weekly IR, alone or in combination with CTX 8mg/kg (3 times/week) were administered to mice. First, we observed that injection of antimiR-9 lentiviral particles once that the tumor mass was already established did not significantly affect subsequent tumor growth, compared to the control counterpart (Fig. 7D, see untreated groups). However, when tumors were treated with RT or RT+CTX, injection of anti-miR9 lentiviral particles significantly improved the efficacy of the treatments (Fig. 7D). Measurement of miR-9 expression in RNA extracted from explanted tumors demonstrated that miR-9 levels were effectively reduced by intra-tumoral injection of antimiR-9 lentiviral particles (Fig. 7E). Analysis on tumor tissue sections also revealed that proliferation (by Ki67 IHC) was decreased and apoptosis, assessed by TUNEL assay, increased in antimiR9-treated tumors, especially in the RT+CTX group (Fig. 7F-G).

Overall, our results suggested that the activation of EGFR/miR-9 axis represents a limitation for the efficacy of RT+CTX. To test whether these *in vitro* findings were also relevant to the human pathology, we first interrogated the TCGA dataset and identified 31 HNSCC patients treated with RT+CTX combination therapy, for which clinical data were available. Using the upper quartile (*i.e.*, > 75,819 reads) as cut-off, we could verify that in this cohort of patients, in line with our previous observations, high miR-9 expression was significantly associated with a poor prognosis ($P = 0.00123$) (Fig. 8A). Next, we set up a droplet digital PCR (ddPCR) approach to finely evaluate miR-9 expression and tried to corroborate these *in silico* data by analyzing samples of tumor biopsies

retrospectively collected from patients treated with RT+CTX in our Institute (n = 16) or at the University Cattolica/Gemelli of Rome (n = 21). After exclusion of two samples because of their low RNA quality, the remaining ones (n = 35) were clustered according to miR-9 expression, using the median expression of miR-9 as cut-off to segregate patients above (miR-9 high) or below (miR-9 low) across the entire cohort. Although the population of patients analyzed was relatively small, the expression of miR-9 represented a very strong predictor of prognosis in this setting (HR 3.75–0.27, P = 0.0382) (Fig. 8B).

Overall, these data support the possibility that miR-9 expression in primary HNSCC tumors could represent a valid biomarker to choose between RT+CTX and RT+CDDP therapeutic strategies in HNSCC patients.

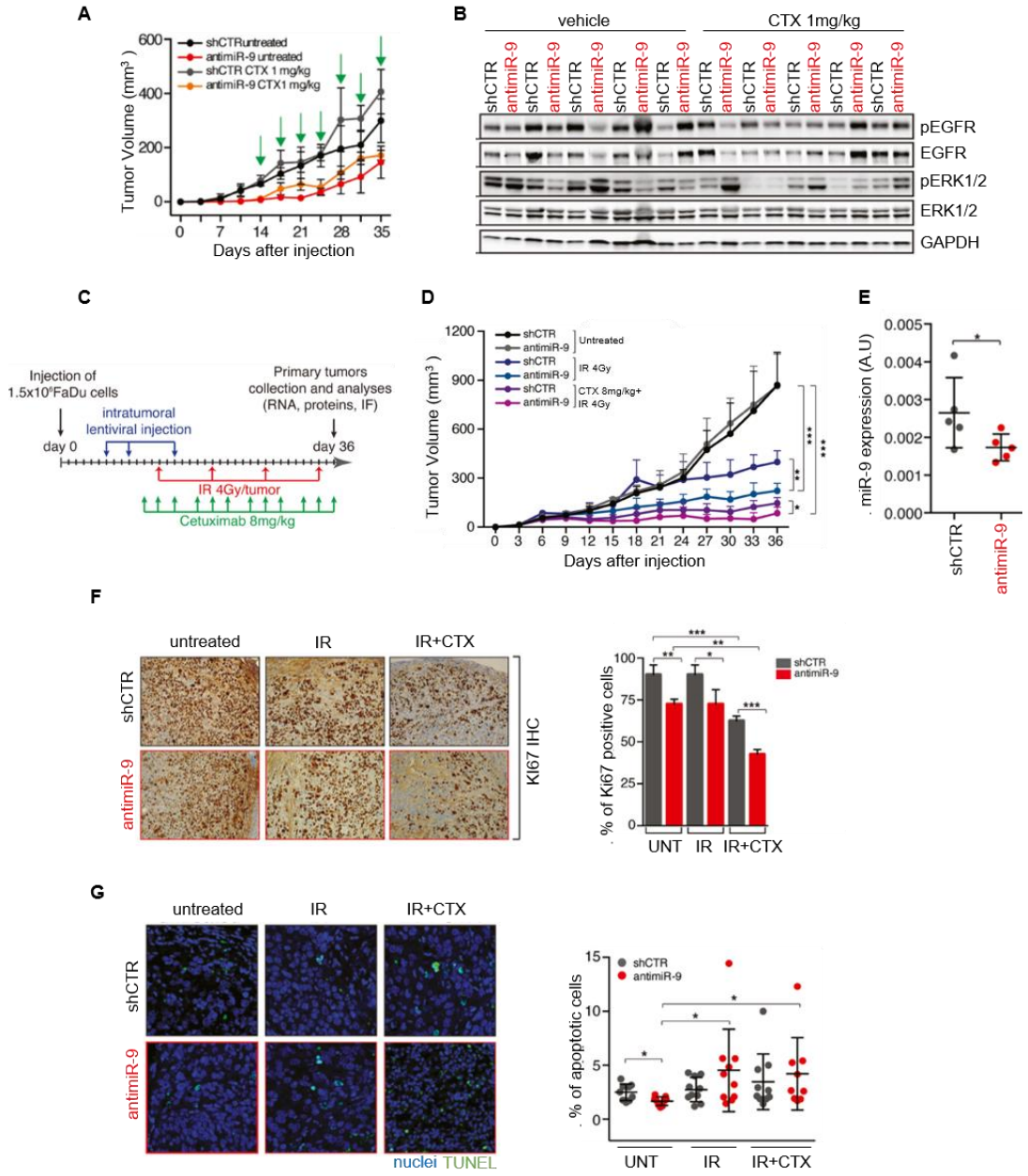

Fig. 7: miR-9 expression regulates and predicts the response to RT+CTX combination therapy. ***A)*** *Graph reporting the tumor volume of mice (n = 5 mice/group) injected in both flanks with shCTR or antimiR-9 FaDu cells and treated with vehicle (untreated) or CTX (1 mg/kg, IP injections) every 3 days for 3 weeks. Data are represented as mean (± SD).* ***B)*** *WB analyses of the indicated proteins expression in tumor explanted from mice described in (A). GAPDH was used as loading control.* ***C)*** *Schema of the in vivo analyses of tumor growth in mice (n = 10/group) injected with FaDu cells. After tumor onset, mice were injected intra-tumoral with high-titer viruses encoding for control or antimiR-9 sequences. After two injections of virus, mice were treated with CTX (IP injections) and RT (4 Gy dose) as indicated and then sacrificed 36 days after IP.* ***D)*** *Graph reports the tumor volume of tumors described in (C) (n = 10 mice/group). Data represent the mean (± SD).* ***E)*** *qRT–PCR of normalized miR-9 expression in tumor treated with shCTR and antimiR-9 lentiviruses FaDu cells as described in (C). Each dot represents a tumor. Data are represented as mean (± SD). In D-E) two-way ANOVA test was used to calculate statistical significance.* ***F)*** *Left, typical images of immunohistochemistry (IHC) to evaluate Ki67 expression in tumors explanted from mice treated as in (C, D). On the right, graph reports the percentage of Ki67-positive cells in tumors. Data are expressed as mean (± SD) of Ki67 percentage counted in five randomly selected fields per tumor, in at least four tumors per group.* ***G)*** *TUNEL assay performed in tumors described in (C-D). Left, typical immunofluorescence images (blue—nuclei, green—TUNEL). On the right, graph reports the percentage of TUNEL-positive cells in tumors. Each dot represents a tumor. Data represent the mean (± SD). In F-G) two-way ANOVA with Sidak's multiple comparison test was used for the statistical significance. .*P < 0.05; **P < 0.01; ***P < 0.001.*

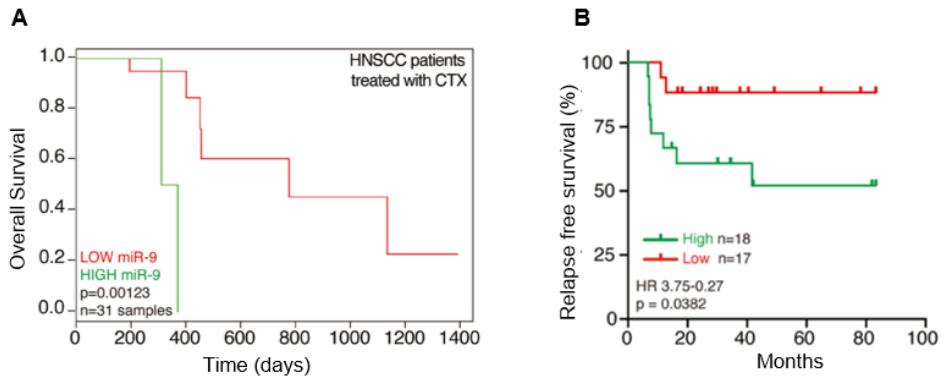

Fig. 8: miR-9 expression in primary HNSCC tumors could be a valid prognostic biomarker. ***A)*** *Kaplan–Mayer curve evaluating the overall survival of HNSCC patients treated with RT+CTX combination included in the TCGA dataset, segregated on the expression of miR-9 in the primary tumor (low expression < 75,819 reads n = 8; high expression ≥ 75,819 reads n = 23). Number of evaluated samples (n) and P value are reported in the graph. Statistical significance was calculated with log-rank test.* ***B)*** *Kaplan–Mayer curve evaluating the progression-free survival of HNSCC patients treated with RT+CTX combination at Centro di Riferimento Oncologico (CRO) of Aviano and at University Cattolica, segregated based on miR-9 expression, evaluated in primary tumors, defined as the expression in above (high expression n = 18) or below (low expression n = 17) the median expression, as defined by ddPCR. The log-rank (Mantel–Cox) test was used for the statistical significance. Hazard ratio (HR) and p value are reported in the graph.*

4.5 miR-9 positively regulates SP1 expression

To understand how miR-9 may regulate the tumorigenic potential and the response to radiotherapy of HNSCC cells, we looked at the expression of the transcription factor SP1. In fact, SP1 expression strongly and positively correlated with the one of miR-9 in HNSCC samples in the TCGA dataset [46] and it is linked to both the acquisition of stem-like properties and the resistance to radiotherapy, altering the DNA damage response (DDR) in different types of cancer, including HNSCC [126,127]

First, we confirmed the observation made in the TCGA dataset in primary HNSCC samples (n = 150), collected in our Institute (Fig. 9A). Then, we investigated whether miR-9 regulated the expression of SP1 in our *in vitro* models. In FaDu antimiR-9 cells, the SP1 mRNA levels decreased (Fig. 9B), while the miR-9 overexpression in CAL27 cells, resulted in a strong upregulation of SP1 mRNA (Fig. 9C). Interestingly, SP1 expression paralleled miR-9 levels in irradiated FaDu cells (Fig. 5C), showing a reduction in both protein and mRNA levels (Fig. 9D-E). Next, we investigated whether SP1 overexpression could be involved in resistance to IR. Using the radiomimetic agent bleomycin, we observed that SP1 overexpression strongly increased resistance to bleomycin in control cells and reverted the IR sensitivity of antimiR-9 FaDu cells (Fig. 9F).

To understand how miR-9 could regulate SP1 expression, we cloned the SP1 promoter in a luciferase reporter vector that allowed us to demonstrate that the abrogation of miR-9 in FaDu cells strongly reduced the SP1 promoter activity supporting that miR-9 positively regulated the transcription of SP1 (Fig. 9G). Then we confirmed these data using CAL27 cells, in which stable miR-9 overexpression markedly increased the promoter activity of SP1 compared to the control (Fig. 9H).

Overall, these data supported that miR-9 may sustain radio-resistance positively regulating SP1 in HNSCC cells

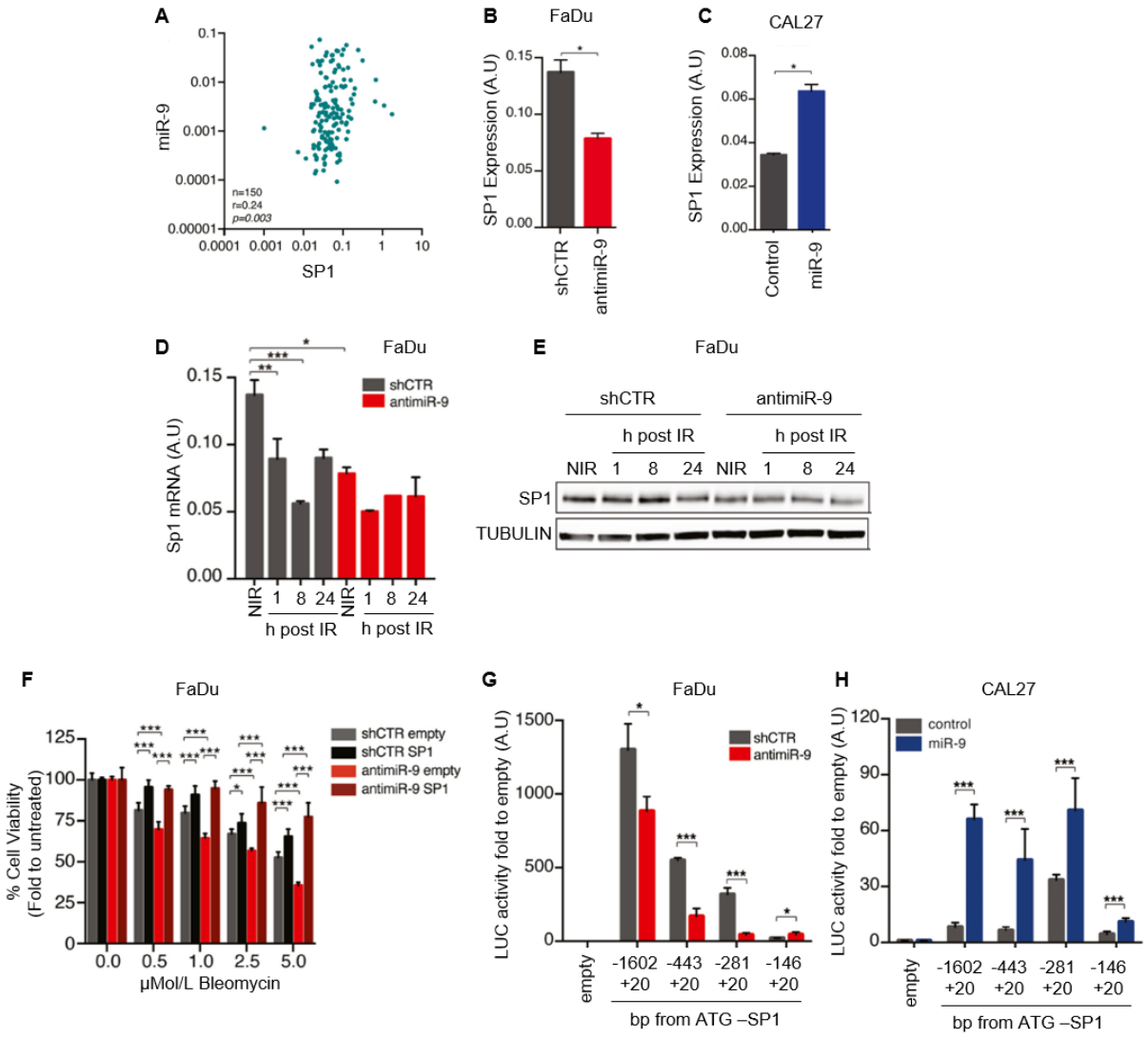

Fig.9: miR-9 positively regulates SP1 expression: A) *Dot plot reporting the correlation of miR-9 and SP1 expression in primary HNSCC samples evaluated by qRT–PCR. The number of analyzed samples (n), the Spearman correlation value (r), and its significance (P) are reported in the graph.* ***B-C)*** *qRT–PCR analyses of SP1 expression in shCTR/antimiR-9 FaDu cells (B) and in Control/miR-9 overexpressing CAL27 cells (C). Data represent the mean (± SD) of three independent experiments performed in duplicate, and unpaired t-test was used to verify the statistical significance.* ***D)*** *qRT–PCR analyses of SP1 normalized expression in FaDu cells not irradiated (NIR) or treated with 5 Gy IR and allowed to repair for the indicated hours. Data are the mean (± SD) of three independent experiment performed in duplicate* ***E)*** *WB analyses of the indicated protein expression in shCTR and antimiR-9 FaDu cells treated as in (D).Tubulin was used as loading control.* ***F)*** *Graph reporting cell viability of shCTR and antimiR-9 FaDu cells, overexpressing or not SP1, and treated with increasing concentration of Bleomycin for 72h and analyzed using the MTS cell viability assay. Data represent the mean (± SD) of three independent experiments each performed in sextuplicate. In D-F) Two-way ANOVA with Sidak's multiple comparison test was used to verify the statistical significance.* ***G-H)*** *Normalized luciferase activity of SP1 promoter fragments in shCTR/antimiR-9 FaDu cells (G) and Control/miR-9 overexpressing CAL27 cells (H). Data represent the mean (± SD) of three independent experiments performed in duplicate, and unpaired t-test was used to verify the statistical significance. A.U. = arbitrary units;*P < 0.05; **P < 0.01; ***P < 0.001.*

4.6 miR-9 indirectly regulates SP1 expression by targeting KLF5

Our luciferase assays showed that miR-9 positively regulated the SP1 transcriptional level (Fig. 9). However, neither SP1 promoter or its 3'-UTR contain any miR-9 seed sites, suggesting that miR-9 affected SP1 transcription indirectly, through the regulation of a different target gene. Using a bioinformatic approach, we recently identified 20 genes representing putative targets of miR-9 and downregulated during HNSCC progression [46]. Among these 20 genes, we particularly focused our attention on KLF5, since several putative KLF5-binding sites are present in the SP1 promoter region and because a KLF5 deletion was already linked to SP1 upregulation in a model of prostate cancer progression [128]. Further, as already mentioned before, KLF5 is a transcription factor and its loss has been involved in several aspects of cancer progression, including tumor initiation.

First, we evaluated KLF-5 expression in response to miR-9 level modulation in our cellular models and observed that inhibition of miR-9 in FaDu cells strongly upregulated KLF5 mRNA and protein expression while miR-9 overexpression in CAL27 cells has the opposite effect and reduced both KLF5 mRNA and protein levels (Fig. 10A-B). Next, we tested whether miR-9 could directly regulate KLF5 expression acting on its 3'-UTR, which contains two different seed sites for miR-9 (Fig. 10C). Luciferase assay in FaDu and CAL27 cells demonstrated that miR-9 silencing significantly increased while miR-9 overexpression reduced the luciferase activity, when both the seed sites are present (WT) and when only one of the 2 seed sites was mutated (Fig. 10D-E). On the contrary, when both the seed sites in 3'UTR of KLF5 were mutated (mut A + B), miR-9 silencing fails to induce the luciferase activity in FaDu cells, compared to the single mutants, and failed to modulate KLF5-driven LUC activity in CAL27 cells (Fig. 10D-E).

Overall, these data demonstrated that KLF5 represents a *bona fide* target of miR-9 in HNSCC cells, as recently reported in HEK293 cells for the rat KLF5 gene [129].

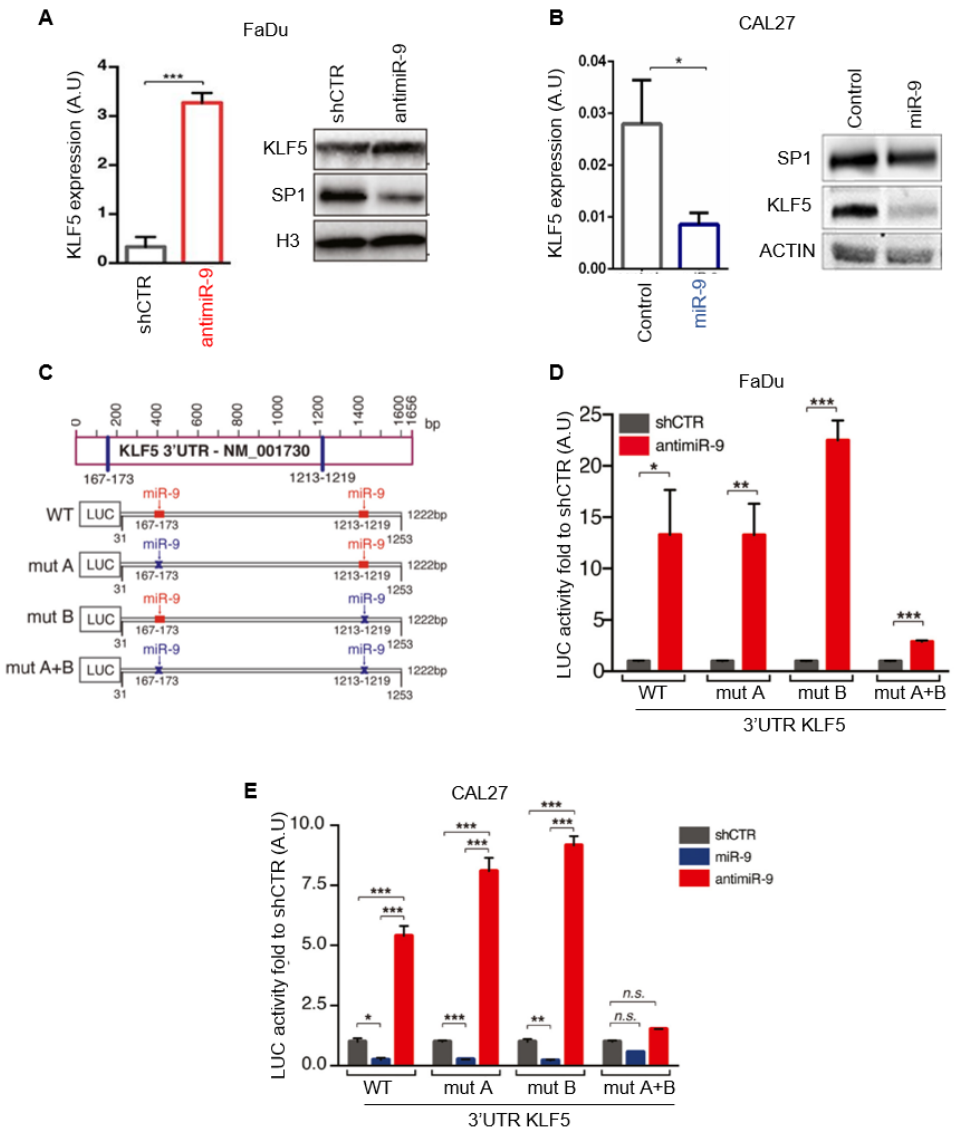

Fig. 10: miR-9 binds and modulates the KLF5 transcription factor expression and activity. ***A)*** *qRT–PCR analyses (left) of KLF5 expression and WB analysis (right) of KLF5 and SP1 expression in shCTR and antimiR-9 FaDu cells. Histone H3 was used as loading control.* ***B)*** *qRT–PCR analyses (left) and WB analysis (right) of KLF5 and SP1 expression in Control and miR-9 overexpressing CAL27 cells. Actin was used as loading control. In A-B) Data represent the mean (± SD) of three independent experiments performed in duplicate, and unpaired t-test was used for the statistical significance.*
C) *Schematic design of the KLF5 3'-UTR. To test the potential miR-9 binding on KLF5 3'-UTR, four vectors were generated: WT (wild type containing both the seed sites), mut A or mut B (mutated for one single binding site) and mut A+B (mutated in both seed site). The seed sites for miR-9-binding are shown in red when it is WT and in blue when it is mutated.* ***D-E)*** *Normalized luciferase activity of WT or mutated KLF5 3'-UTR in FaDu (shCTR/antimiR-9) cells and in CAL27 (shCTR miR-9 overexpressing and antimiR-9) cells, as indicated. Data represent the mean (± SD) of three independent experiments performed in duplicate and two-way ANOVA with Sidak's multiple comparison test was used to verify the statistical significance. A.U. = arbitrary units;*P < 0.05; **P < 0.01; ***P < 0.001.*

Next, we tested whether KLF5, in turn, could regulate SP1 expression in HNSCC.

Overexpression of KLF5, in either FaDu or CAL27 cells, resulted in a strong down-regulation of SP1 mRNA and protein levels (Fig. 11A-C-E). Then, by luciferase assay, we confirmed the reduced SP1 promoter activity after KLF5 overexpression, in both the cell lines (Fig. 11B-D). Moreover, Chromatin ImmunoPrecipitation (ChIP) assay on FaDu and CAL27 cells confirmed that endogenous KLF5 binds to the SP1 promoter on four possible binding sites, located between base –253 and –1602 from the ATG (Fig. 11F-G).

Altogether, data collected strongly supported that miR-9 regulates SP1 by targeting KLF5 and suggested that this could be the way by which miR-9 could participate to the tumorigenic potential of HNSCC cells and, eventually, to the resistance to EGFR blockade.

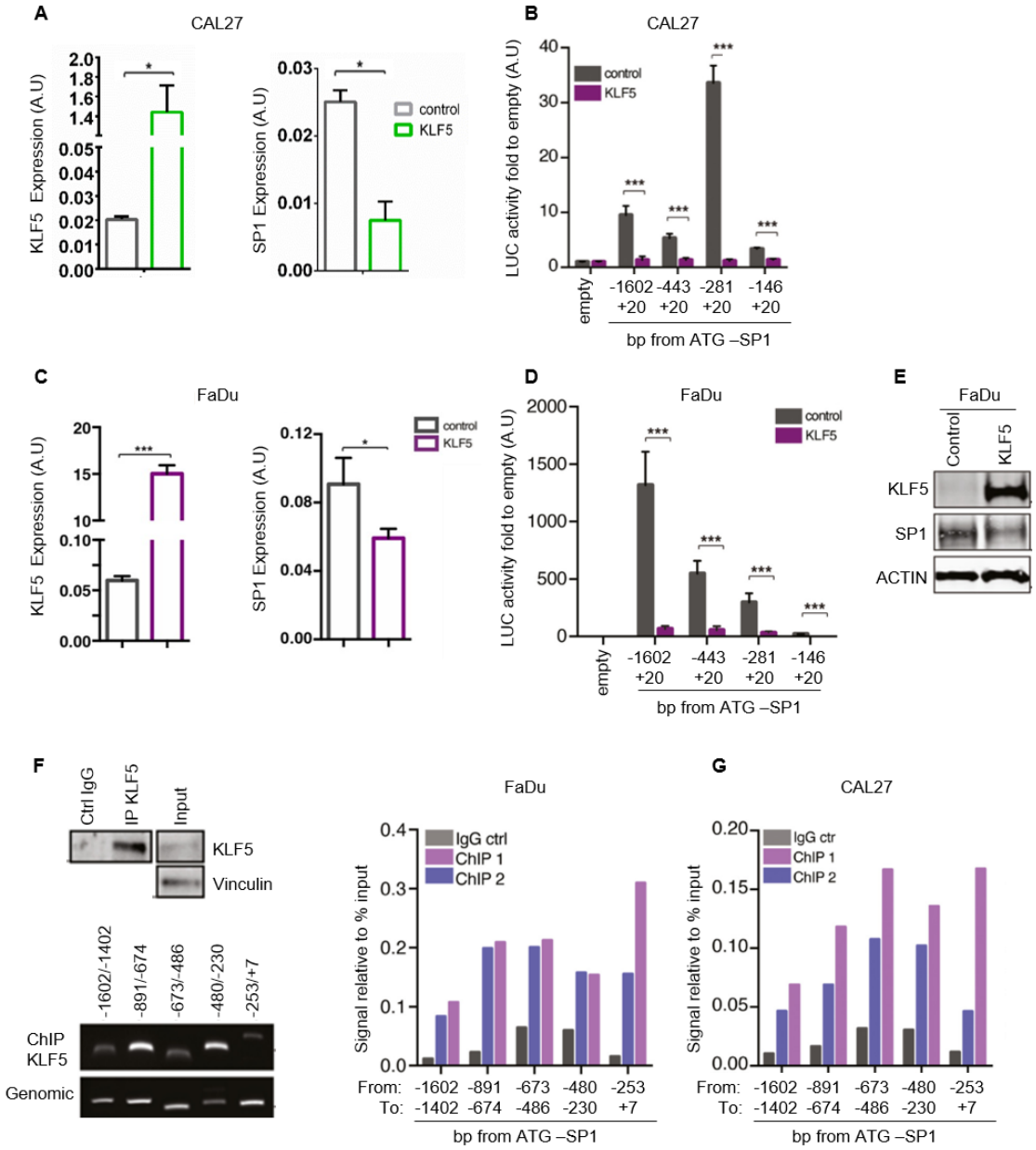

Fig. 11: KLF5, modulated by miR-9, regulates SP1 expression in HNSCC. A-C) *qRT-PCR analyses of normalized KLF5 (left) and SP1 (right) expression in CAL27 (A) and in FaDu cells (C) transfected with control or KLF5 vector.* ***B, D)*** *Normalized Luciferase activity of SP1 promoter fragments in CAL27 and FaDu cells transfected with control or KLF5 vectors, as indicated. In A-B-C-D) data represent the mean (± SD) of three independent experiments performed in duplicate, and unpaired t-test was used for the statistical significance.* ***E)*** *WB analyses of the KFL5 and SP1 expression in FaDu cells transfected as indicated.* ***F)*** *Chromatin immunoprecipitation (ChIP) assay performed on FaDu cells. Upper left panel shows WB analysis reporting KLF5 expression in the immunoprecipitation achieved using anti-KLF5 or control (IgG) antibodies used in the ChIP assay. Vinculin was used as loading control. Bottom left panel shows a typical image of amplified PCR fragments using ChIP DNA or genomic DNA, as indicated. Right, graph reports the KLF5 binding to the indicated region of SP1 promoter expressed as signal relative to input in two independent immunoprecipitations (ChIP1 and ChIP2) performed in FaDu cells. IgG was used as negative control on the same chromatin.* ***G)*** *KLF5 binding to the indicated region of SP1 promoter expressed as signal relative to input in two independent immunoprecipitations (ChIP1 and ChIP2) performed in CAL27 cells. IgG was used as negative control on the same chromatin.*
*A.U. = arbitrary units; *P < 0.05; **P < 0.01; ***P < 0.001.*

4.7 TP53 status in HNSCC dictates different KLF5 impact on SP1 expression

TP53 mutations are relatively early events in squamous cell carcinogenesis, mutually exclusive with HPV infection, even though they are not sufficient for the development of human HNSCC.
Moreover, TP53 represents also one of the molecular switches of the KLF5 activity that, in presence of a mutant p53, KLF5 predominantly acts as a tumor suppressor in SCC.
For these scientific evidences, we asked whether KLF5 activity on SP1 expression could be also dependent on p53 status, possibly leading to different clinical outcomes and different response to therapy between the HNSCC HPV+ patients, who are TP53 wild type, and HPV− patients, who almost invariantly harbor p53 mutations. Accordingly, we observed that in CAL27 cells, mutated for p53, KLF5 strongly downregulate SP1 expression at both RNA (Fig. 11A) and protein level likely acting on its promoter as demonstrated by luciferase assay in a dose-response experiment (Fig. 12A). On the contrary, in UMSCC74B cells, which harbor a WT TP53 gene, KLF5 overexpression leads to an increase of SP1 protein and RNA level and promoter activity (Fig. 12B). Finally, we used the TP53 null SCC9 cells in which we overexpressed KLF5 alone or together with vectors encoding for WTp53 or MUTp53. The results from these analyses confirmed that overexpression of KLF5 downregulated SP1 expression at both RNA and protein level when p53 was absent or mutated, and had the opposite effect when WTp53 was expressed (Fig. 12C). A luciferase assay in a p53 null context confirmed that KLF5 inhibited SP1 promoter activity, overall acting as a tumor suppressor when p53 WT protein is not expressed. Interestingly, western blot analyses demonstrated that overexpression of MUTp53 alone was not sufficient to alter the SP1 expression that decreases only when MUTp53 is expressed together with KLF5.
To confirm these data, using a lentiviral shRNA approach we generated KLF5-silenced CAL27 and UMSCC74B stable cell pools. Strikingly, KLF5 silencing in a WTp53 context (UMSCC74B cells) led to a strong decrease in SP1 protein levels compared to the shCTR counterpart, while in MUTp53 context (CAL27 cells), SP1 expression after KLF5 silencing remained stable and substantially equal to the one of control cells (Fig. 13A). Based on the notion that miR-9 overexpression, by down regulating KLF5 in cells expressing MUTp53 (FaDu and CAL27) markedly increased the SP1 level compared to the control (Fig. 9), we tested its effect in UMSCC74B cells (WTp53). by binding and down modulating KLF5, led to a strong decrease of SP1 (Fig. 13B).

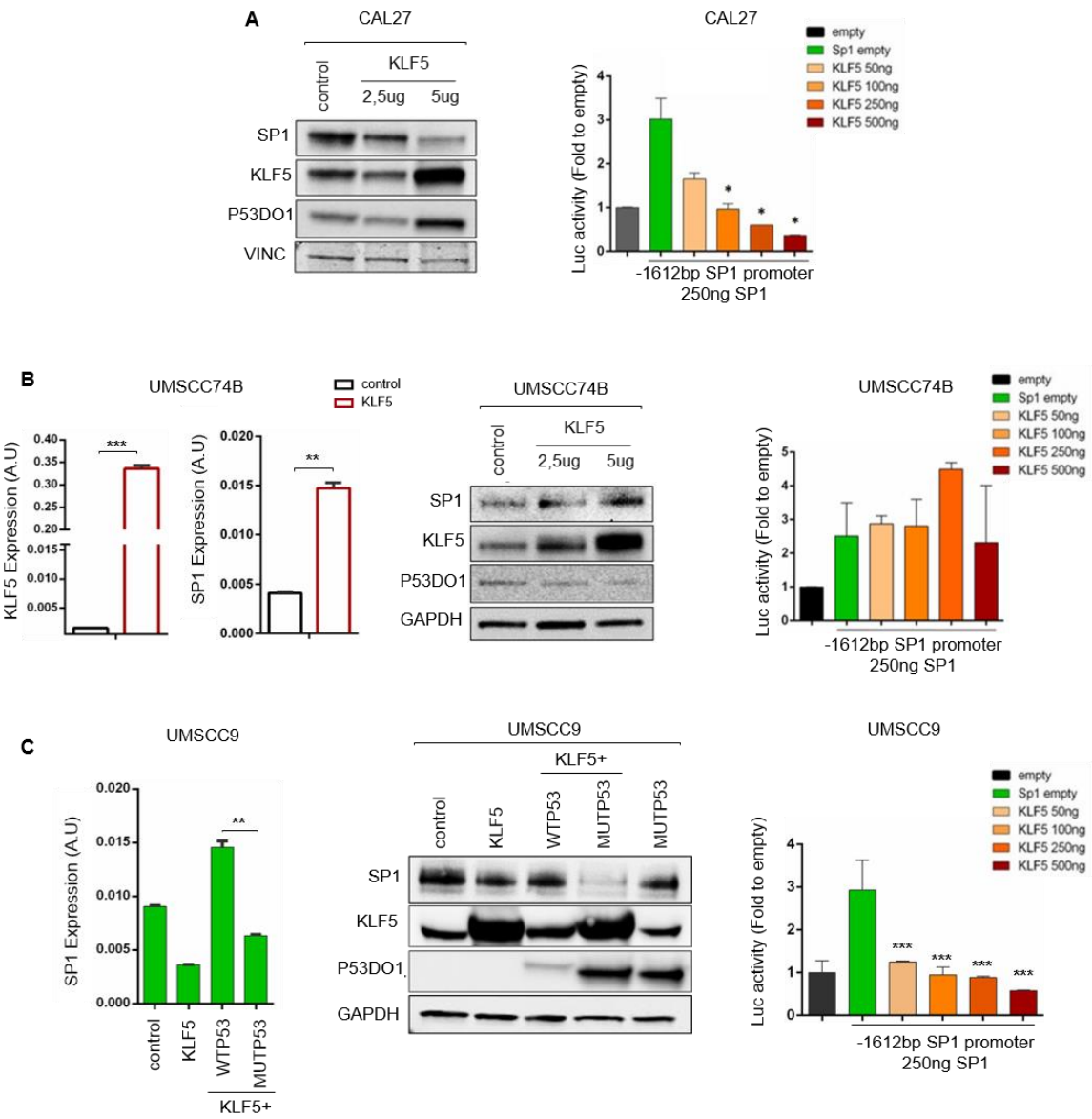

Fig. 12: KLF5 displays different activity on SP1, depending from p53 contexts. A) *Left, WB analyses of the indicated proteins in CAL27 cells transfected with control vector or with KLF5 vector as indicated. On the right, normalized luciferase activity of SP1 promoter in CAL27 cells transfected with control or SP1 vector or KLF5 vectors in increasing doses, as indicated.* ***B)*** *Left, qRT-PCR analyses of normalized KLF5 and SP1 expression in UMSCC74B cells transfected with KLF5 vector. In the middle, WB analyses of the indicated proteins expression in UMSCC74B cells transfected as in A). On the right, normalized luciferase activity of SP1 promoter in UMSCC74B cells transfected as in (A).* ***C)*** *Left, qRT-PCR analyses of normalized SP1 expression in SCC9 cells transfected with empty, KLF5 vector or co-transfected with KLF5 plus p53WT and MUT vectors. Middle, WB analysis of the indicated proteins in SCC9 cells transfected as indicated. On the right, normalized Luciferase activity of SP1 promoter in SCC9 cells transfected as in (A). In A-B-C) data represent the mean (± SD) of three independent experiments performed in duplicate, and unpaired t-test was used for the statistical significance. For WB analysis GAPDH was used as loading control.*P ⩽0.05; **P ⩽ 0.01; ***P ⩽ 0.00.1.*

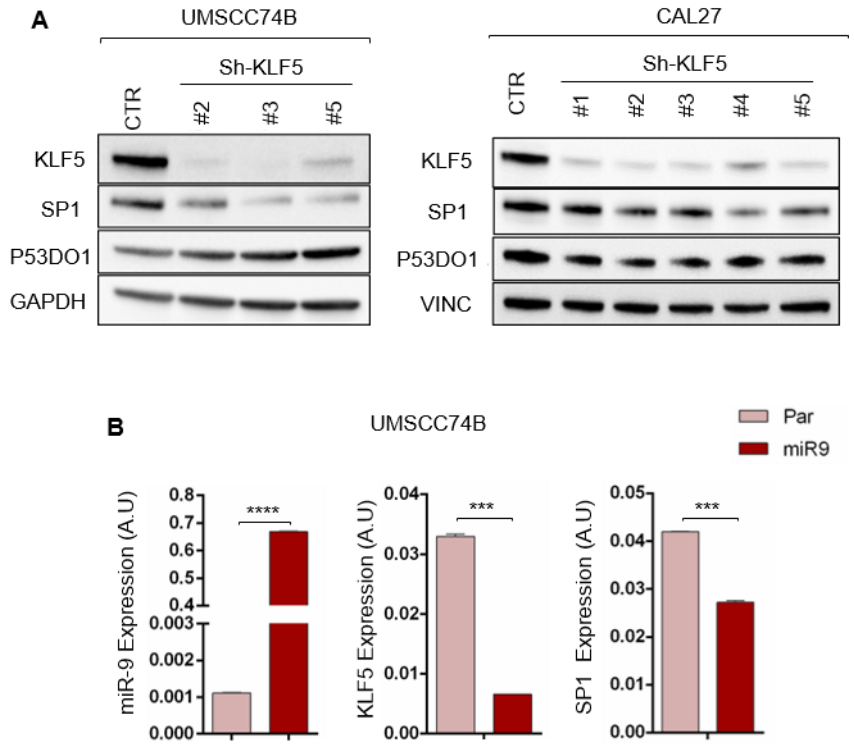

Fig. 13: Loss of KLF5 affects SP1 expression depending on p53 context. A) *WB analyses of the indicated proteins in UMSCC74B (left) and in CAL27 (right) pools stably silenced for KLF5.* ***B)*** *qRT-PCR analyzes of normalized miR-9, KLF5 and SP1 expression in UMSCC74B cells transfected with miR-9 vector.*

Many evidences confirm a strong crosstalk between SP, KLF and p53 transcription factors, commonly altered in HNSCC. Moreover, it is well known in literature that SP1 and KLF5 are able to cooperate with both wild type and mutated p53, thereby modulating the activity of many downstream proteins involved in several biological processes, switching their activities depending on p53 status [53,51]. To assess whether the crosstalk between KLF5, SP1 and p53 played a role also in our context, we first evaluated their reciprocal interactions under different conditions. Co-Immunoprecipitation assay (Co-IP) showed that KLF5 binds both SP1 and p53 in our HNSCC cellular lines, both when p53 is wild type and mutated. These evidences were confirmed also by IP p53 and looking at its interaction with both KLF5 and SP1 (Fig. 14A).

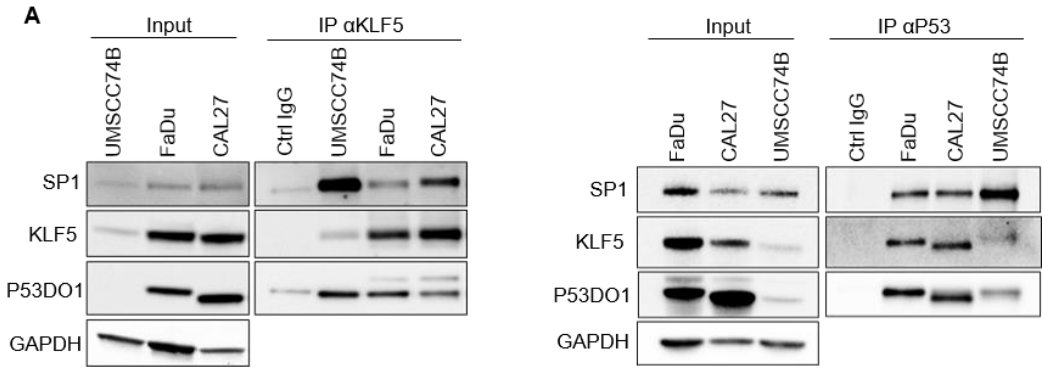

Fig. 14: KLF5/p53/SP1 directly interact with each other, independently from p53 status. A) *Co-Immunoprecipitation analyses of endogenous KLF5, SP1 and p53 proteins in FaDu, CAL27 and UMSCC74B cells. Input shows the expression of the indicated proteins in the correspondent lysates; Ctrl IgG represents the control IP using an unrelated antibody. Data represent the mean (± SD) of three independent experiments performed in duplicate, and unpaired t-test was used for the statistical significance. For WB analysis, GAPDH and Vinculin were used as loading control. *P ⩽0.05; **P ⩽ 0.01; ***P ⩽ 0.00.1.*

4.8 KLF5/p53/SP1 axis modulates response to therapy of HNSCC, *in vitro*

The data collected so far showed that in the context of TP53 mutated cells KLF5 acted as tumor suppressor leading to decreased SP1 expression and increased sensitivity to radiotherapy and/or radiomimetic drugs and CTX. Conversely, in TP53 WT cells it induced the expression of SP1 raising the possibility that it could differently affect the response to therapies.

To evaluate this possibility, we first treated WTp53 (UMSCC74B) and MUTp53 (CAL27) HNSCC cell lines with the radiomimetic drug bleomycin, used as single agent or in combination with CTX. Interestingly, both treatments seemed to be more effective in MUTp53 CAL27 cells, compared to WTp53 UMSCC74B (Fig. 15A). Accordingly, the expression of γH2AX, marker of DNA damage, was significantly higher in CAL27 than in UMSCC74B, confirming and giving an explanation to the fact that the MUTp53 cells were more sensitive to treatments compared to WTp53 counterpart (Fig. 14B).

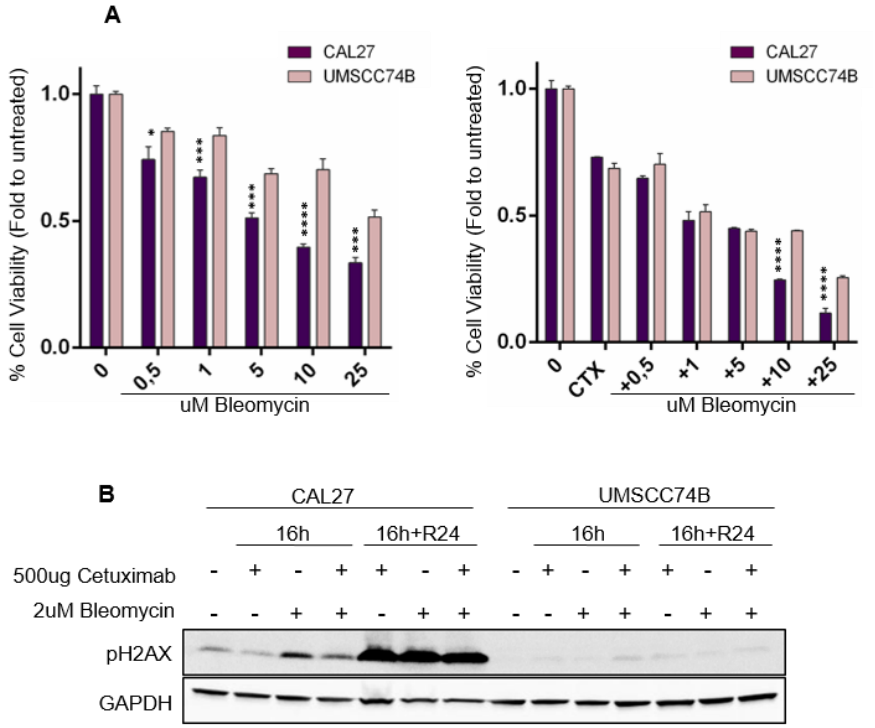

Fig. 15: HNSCC cell lines respond differently to the treatments, depending on p53 status. A) *Graphs reporting cell viability of CAL27 cells and UMSCC74B cells treated with increasing concentration of Bleomycin as single agent (left) and in combination with 500ug of CTX (right) for 72h and analyzed using the MTS cell viability assay. Data represent the mean (± SD) of three independent experiments each performed in sextuplicate. Unpaired t-test was used to calculate the statistical significance per each dose of drugs* ***B)*** *WB analysis of the indicated protein expression in CAL27 and UMSCC74B cells treated with 500ug of CTX and/or 2uM of Bleomycin after 16 hours (16h) or after 16h + 24 hours of release (16h+24R). GAPDH was used as loading control. *P < 0.05; **P < 0.01; ***P < 0.001.*

Next, we looked at their sensitivity to the treatments after modulating KLF5 expression.

When treated with bleomycin and bleomycin + CTX, KLF5 silenced CAL27 cells (MUTp53), were more resistant to both treatments compared to the shCTR counterpart (Fig. 15A-B) On the contrary, the same treatment conditions re-sensitized the shKLF5 UMSCC74B cells, WT for p53 (Fig. 15C).

To further verify whether KLF5 could affect the RT-induced DNA damage response (DDR), we next assessed the expression of γH2AX (DNA damage marker), both in CAL27 and UMSCC74B, after silencing KLF5. We irradiated cells and allowed them to repair the DNA damage for 1, 4 and 24 hours and showed that γH2AX level paralleled the trend of response to the treatments of the two cell lines. Indeed, it was significantly higher in UMSCC74B KLF5 silenced cells than in CAL27 KLF5 silenced ones (Fig. 15D). Moreover, in UMSCC74B cells a strong γH2AX expression was observed when KLF5 expression was lower than controls.

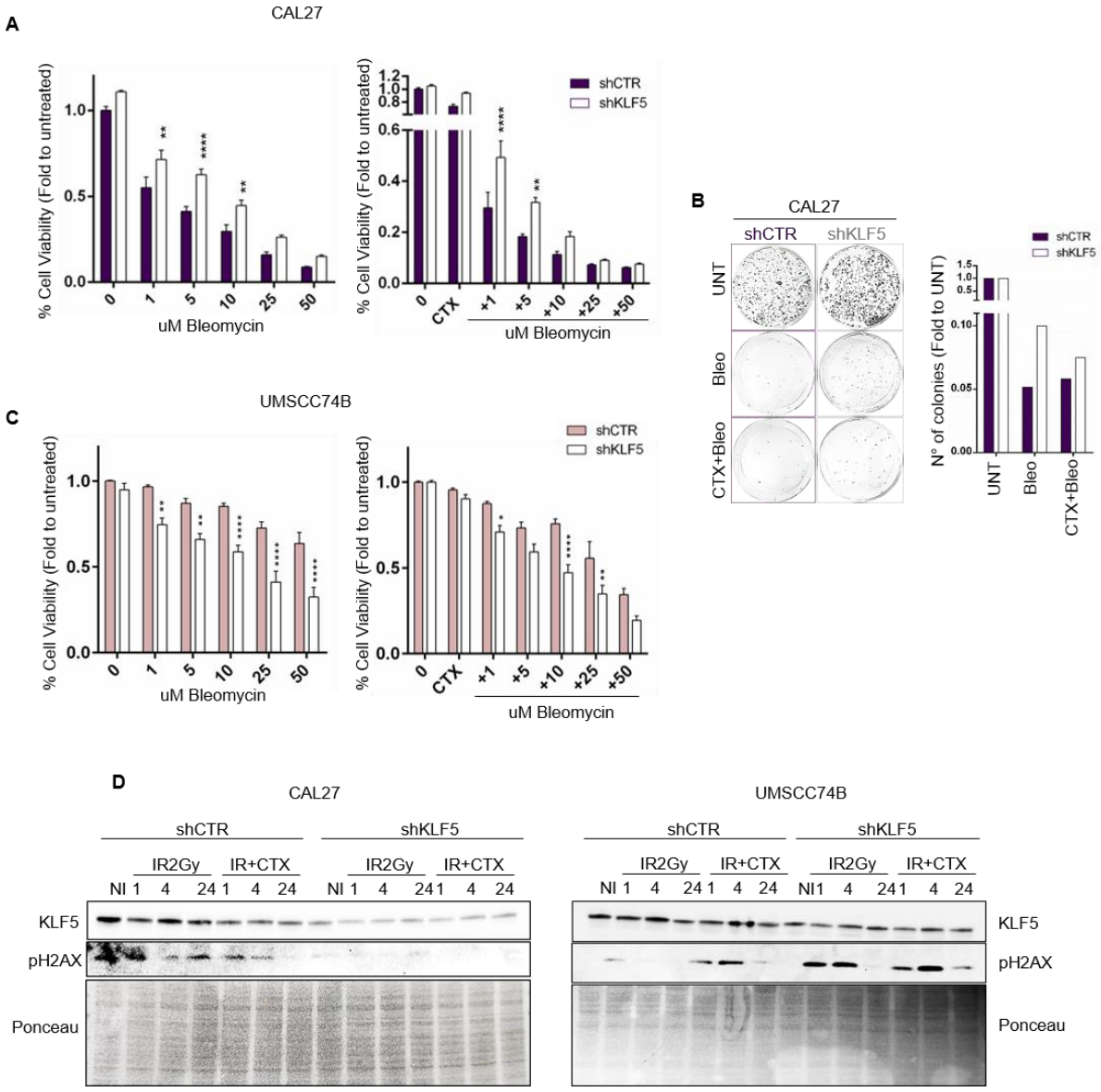

Fig.15: Loss of KLF5 affects the response to therapy of HNSCC cells. A-C) *Graphs reporting cell viability of CAL27 shCTR and shKLF5 cells (A) and UMSCC74B shCTR and shKLF5 cells (C) treated with increasing concentration of Bleomycin as single agent (left) and in combination with 500ug of CTX (right) for 72h and analyzed using the MTS cell viability assay. Data represent the mean (± SD) of three independent experiments each performed in sextuplicate. Unpaired t-test was used to calculate the statistical significance per each dose of drugs.* ***B)*** *Clonogenic assays of CAL27 cells (shCTR and shKLF5) untreated (UNT) or treated with 2uM of Bleomycin (Bleo) as single agent and in combination with 500ug of CTX. Left, typical images of cell clones are show. On the right, the graph reports the number of survived colonies (folded to UNT).****D)*** *WB analyses of the indicated protein expression in CAL27 cells (shCTR and shKLF5) and UMSCC74B cells (shCTR and shKLF5) NI or treated with 2Gy IR and/or in combination with CTX allowed to repair for 1-4-24 hours. Ponceau was used as loading control.*P < 0.05; **P < 0.01; ***P < 0.001.*

Overall these findings, although they need to be corroborated using both animal models and patients' specimens, support the possibility that KLF5 transcription factor differently impacts in the DNA damage response following RT alone or RT+CTX depending on p53 status. We will could propose that KLF5 may act as prognostic/predictive biomarkers and, possibly, therapeutic targets for HNSCC TP53 wt/HPV+ patients who are still unable to benefit from the RT+CTX treatment.

5. DISCUSSION

Loco-regional and distant relapses are frequent events in HNSCC patients, mainly due to the advanced disease stage at the diagnosis. Unfortunately, the appearance of recurrence strongly influences patients' outcome and represents a common unfavorable prognostic event [2,3].

Advanced HNSCC also displays the worse response to standard of care, even when a very aggressive (and highly toxic) chemotherapeutic schedule is administered [4].

TP53 mutations are early events in squamous cell carcinogenesis, mutually exclusive with HPV infection, even though they are not sufficient for the development of human HNSCC. Not surprisingly, these two types of HNSCC tumors, TP53mut/HPV− and TP53wt/HPV+, have a very different molecular and clinical behavior and respond very differently to therapies. In particular, the de-escalation treatment based on the combination of Radiotherapy (RT) with Cetuximab (CTX) has demonstrated some encouraging result only in TP53mut/HPV− HNSCC patients [1,100]. However, also patients belonging within this group displayed substantial differences in the response to RT+CTX, but prognostic and/or predictive markers of efficacy are missing, eventually resulting in many patients treated with disappointing results and unnecessary toxicities.

Thus, many clinical challenges need to be faced for a better management of HNSCC patients. First, the identification of biomarkers able to stratify patients in low- and high-risk of recurrence and, further, predict who will respond to RT+CTX and those who will, instead, need RT+chemotherapy. Moreover, discovering new potential druggable targets to improve and personalize therapy is another urgent clinical need for all advanced HNSCC patients.

This PhD project dealt with these unmet clinical needs and aimed at identifying the key molecular players driving aggressiveness in TP53mut/HPV− HNSCC, in order to discern both biomarkers of response to therapies and, possibly, new targetable molecules. We identified a signaling axis, involving miR-9, KLF5 and SP1 that connects the tumor stem-like features of HNSCC with the response to therapy, in a TP53 dependent manner. The central node of this pathway is miR-9 that can indirectly control SP1 transcriptional activity through KLF5 and, thereby, regulate the response to DNA damage and the biological behavior of HNSCC cells.

Our data demonstrate that miR-9 transcription is rapidly induced by serum (1–2h) in HNSCC cells, supporting the possibility that immediate-early gene(s), such as c-Myc and EGFR, activated in response to mitogenic stimuli, including EGF [130], are involved in the regulation of its promoter activity.

In vitro, high miR-9 levels conferred to HNSCC cells a higher tumorigenicity, acquisition of stem-like properties with higher self-renewal capabilities, resistance to DNA damage following irradiation and resistance to RT+CTX treatment. *In vivo*, activation of EGFR/miR-9 axis limited the efficacy of

RT+CTX combination treatment. Moreover, in primary HNSCC, both from the TCGA datasets and from patients "real world" samples collected and analyzed in our lab, high miR-9 levels predicted poor prognosis in patients treated with RT+CTX.

Our molecular data pointed to the possibility that miR-9 regulated the tumorigenic potential and the RT response of HNSCC cells acting on the activity of the transcription factor SP1, known to be involved in both the acquisition of stem-like properties and the resistance to radiotherapy, altering the DNA damage response in different types of cancer, including HNSCC [126,127].

Accordingly, SP1 expression strongly and positively correlated with miR-9, both in HNSCC samples from the TCGA dataset [46] and in our *in vitro* models and its overexpression increased the resistance to DNA damage, after both bleomycin and RT treatment. At mechanistic level, we found that miR-9 affects SP1 transcription indirectly, through the regulation of a different target gene, *i.e.* KLF5. Through detailed experimental study, we discovered that miR-9 can directly down-modulate KLF5 expression, by targeting two seed sites in its 3'UTR. Then, in turn, KLF5 regulates SP1 by acting on its promoter activity.

It has been proposed that KLF5 can act as either tumor suppressor or oncogene, depending on the tissue and cellular context and that p53 could represent one of the molecular switches of KLF5 activity [79]. Interestingly, TP53 mutations are generally mutually exclusive with HPV infection in HNSCC, and these two types of tumors (TP53mut/HPV− and TP53wt/HPV+) respond very differently to therapies, particularly to CTX+RT [4,86]. Two recent clinical trials have demonstrated that RT+CTX is not a feasible therapeutic opportunity in HPV+ HNSCC patients, although negativity for HPV cannot be considered a straightforward predictor of response to CTX, as well [24,25].

Given these evidences, we asked whether KLF5 activity on SP1 expression could be also dependent on p53 status, possibly leading to different clinical outcomes and different response to therapy between the HNSCC HPV+ patients, who are p53 wild type, and HPV− patients, who almost invariantly harbor p53 mutations. Accordingly, our data demonstrated that miR9/KLF5 axis regulation on SP1 works in concert with p53 status. When p53 was mutated, KLF5 downregulated SP1 and, then, miR-9 overexpression led to increase of SP1 transcription and expression, unleashing its tumorigenic transcriptional activities and affecting the cellular sensitivity to RT+CTX. When p53 was WT, KLF5 led to opposite effects, upregulating SP1 at both expression level and transcriptional activity. Moreover, down modulation of KLF5 in HNSCC cells exerted opposite effects on SP1 expression, also affecting the responsiveness to RT+CTX treatment, in a p53-dependent manner.

Altogether, our data support the possibility that in a subset of TP53-mut/HPV− HNSCC, the expression of miR-9 could promote tumor growth and the resistance to therapies. In this setting, we can expect two scenarios: in miR-9 low tumors, the addition of CTX to RT, *via* blockage of the EGFR

signaling pathway, will further decrease miR-9 expression, eventually contributing to the effectiveness of the RT treatment; in miR-9 high tumors, the EGFR signaling pathway inhibition by CTX is not sufficient to dampen the miR-9/KLF5/SP1 axis and HNSCC will resist to treatments and eventually progress. In a TP53 wild-type context, our data suggest that KLF5 down-regulation, either *via* miR-9 or by other mechanisms, will have little effect on SP1 oncogenic pathway, therefore contributing to the resistance to CTX+RT therapeutic strategy.

The newly identified axis, linking EGFR activation to SP1 expression *via* miR-9 and KLF5, seems to represent a robust biomarker of CTX activity. On these bases, the evaluation of miR-9 expression in primary tumor biopsies, or, possibly, in the saliva of HNSCC patients may represent a feasible strategy to stratify patients and assign them to the most effective combination therapy, between RT+CTX and RT+chemotherapy.

In addition, our data suggest that KLF5, p53 and SP1, possibly acting as a transcriptional complex, can modulate the expression and activity of a wide range of genes, differently involved in tumor development and progression.

The significant effect that we observed when SP1 and KLF5 were down modulated and the critical role of miR-9 in promoting resistance to both radiotherapy and EGFR-targeted therapy strongly encourages us to try to translate our findings to the clinic. Indeed, our data are of potential immediate translational relevance, since the evaluation of both TP53 status and miR-9 expression in primary HNSCC biopsies is feasible and easily applicable to the clinical setting. Moreover, due to their involvement in many biological cellular processes, miR-9, p53, SP1 and KLF5 could be proposed as potential biomarkers and/or therapeutic targets in many types of cancer, not only HNSCC, thus widening the potential implications of our study.

We are aware that our study has several limitations that should be taken into account. For instance, the effect of SP1 and KLF5 modulation, affecting the responsiveness to RT+CTX treatment according the p53 status, has been, so far, only evaluated *in vitro*. Thus, *in vivo* experiments and more in-depth studies of their molecular mechanisms and molecular partners in different contexts are needed to better understand how their functions could be optimally modulated and to corroborate their potential use in the clinic. At this regard, in fact, inhibition of KLF5 by administrating drugs or other small molecules, in combination with the anti-EGFR therapy or RT, could represent a new therapeutic strategy that may be effective, especially for TP53wt/HPV+ HNSCC patients, who do not benefit from the RT+CTX treatment.

Altogether, dissecting the role of this new mir-9/KLF5/TP53/SP1 axis have allowed to unveil interesting insights to a better understanding of the mechanism by which WTp53 and MUTp53 affect gene expression. This new understanding may help identifying novel molecular partners, such as

KLF5 and SP1, that contribute to its gain-of-function activities, and that could be more easily targetable compared to p53.

6. REFERENCES

1. Leemans, C. R., Braakhuis, B. J. M. & Brakenhoff, R. H. The molecular biology of head and neck cancer. *Nat. Rev. Cancer* **11**, 9–22 (2011).

2. Bray, F. *et al.* Global cancer statistics 2018: GLOBOCAN estimates of incidence and mortality worldwide for 36 cancers in 185 countries. *CA. Cancer J. Clin.* **68**, 394–424 (2018).

3. Johnson, D. E. *et al.* Head and neck squamous cell carcinoma. *Nat. Rev. Dis. Prim.* **6**, (2020).

4. Leemans, C. R., Snijders, P. J. F. & Brakenhoff, R. H. The molecular landscape of head and neck cancer. *Nat. Rev. Cancer* **18**, 269–282 (2018).

5. Canning, M. *et al.* Heterogeneity of the head and neck squamous cell carcinoma immune landscape and its impact on immunotherapy. *Front. Cell Dev. Biol.* **7**, 1–19 (2019).

6. Chung, C. H. & Gillison, M. L. Human papillomavirus in head and neck cancer: Its role in pathogenesis and clinical implications. *Clin. Cancer Res.* **15**, 6758–6762 (2009).

7. Ragin, C. C. R. & Taioli, E. Survival of squamous cell carcinoma of the head and neck in relation to human papillomavirus infection: Review and meta-analysis. *Int. J. Cancer* **121**, 1813–1820 (2007).

8. Moody, C. A. & Laimins, L. A. Human papillomavirus oncoproteins: Pathways to transformation. *Nat. Rev. Cancer* **10**, 550–560 (2010).

9. Schache, A. Human Papillomavirus and Survival of Patients with Oropharyngeal Cancer. *50 Landmark Pap. every Oral Maxillofac. Surg. Should Know* 31–36 (2020). doi:10.1201/9780429288036-6

10. Lawrence, M. S. *et al.* Comprehensive genomic characterization of head and neck squamous cell carcinomas. *Nature* **517**, 576–582 (2015).

11. Poeta, M. L. *et al.* TP53 Mutations and Survival in Squamous-Cell Carcinoma of the Head and Neck . *N. Engl. J. Med.* **357**, 2552–2561 (2007).

12. Chien, H. T., Cheng, S. De, Liao, C. T., Wang, H. M. & Huang, S. F. Amplification of the EGFR and CCND1 are coordinated and play important roles in the progression of oral squamous cell carcinomas. *Cancers (Basel).* **11**, 1–12 (2019).

13. Stransky, N. *et al.* The mutational landscape of head and neck squamous cell carcinoma. *Science (80-.).* **333**, 1157–1160 (2011).

14. Bernier, J. *et al.* Postoperative irradiation with or without concomitant chemotherapy for locally advanced head and neck cancer. *Cancer/Radiotherapie* **9**, 203–204 (2005).

15. Cooper, J. S. *et al.* Postoperative ccrt rtog 9501. *N Engl J Med* **350**, 1937–1981 (2004).

16. Bauml, J. M. *et al.* Cisplatin Every 3 Weeks Versus Weekly with Definitive Concurrent Radiotherapy for Squamous Cell Carcinoma of the Head and Neck. *J. Natl. Cancer Inst.* **111**, 490–497 (2019).

17. Moreira, J., Tobias, A., O'Brien, M. P. & Agulnik, M. Targeted Therapy in Head and Neck Cancer: An Update on Current Clinical Developments in Epidermal Growth Factor Receptor-Targeted Therapy and Immunotherapies. *Drugs* **77**, 843–857 (2017).

18. Kriegs, M. *et al.* Analyzing expression and phosphorylation of the EGF receptor in HNSCC. *Sci. Rep.* **9**, 1–8 (2019).

19. Khan, H. *et al.* Correlation between expressions of Cyclin-D1, EGFR and p53 with chemoradiation response in patients of locally advanced oral squamous cell carcinoma. *BBA Clin.* **3**, 11–17 (2015).

20. Hintelmann, K., Kriegs, M., Rothkamm, K. & Rieckmann, T. Improving the Efficacy of Tumor Radiosensitization Through Combined Molecular Targeting. *Front. Oncol.* **10**, 1–19 (2020).

21. Mehra, R., Cohen, R. B. & Burtness, B. A. The role of cetuximab for the treatment of squamous cell carcinoma of the head and neck. *Clin. Adv. Hematol. Oncol.* **6**, 742–750 (2008).

22. Fasano, M. *et al.* Head and neck cancer: the role of anti-EGFR agents in the era of immunotherapy. *Ther. Adv. Med. Oncol.* **13**, 10–20 (2021).

23. Taberna, M., Oliva, M. & Mesía, R. Cetuximab-containing combinations in locally advanced and recurrent or metastatic head and neck squamous cell carcinoma. *Front. Oncol.* **9**, (2019).

24. Bonner, J. A. *et al.* Radiotherapy plus cetuximab for locoregionally advanced head and neck cancer: 5-year survival data from a phase 3 randomised trial, and relation between cetuximab-induced rash and survival. *Lancet Oncol.* **11**, 21–28 (2010).

25. Mehanna, H. *et al.* Radiotherapy plus cisplatin or cetuximab in low-risk human papillomavirus-positive oropharyngeal cancer (De-ESCALaTE HPV): an open-label randomised controlled phase 3 trial. *Lancet* **393**, 51–60 (2019).

26. Rieckmann, T. & Kriegs, M. The failure of cetuximab-based de-intensified regimes for HPV-positive OPSCC: A radiobiologists perspective. *Clin. Transl. Radiat. Oncol.* **17**, 47–50 (2019).

27. Anglicheau, D., Muthukumar, T. & Suthanthiran, M. MicroRNAs: Small RNAs with big effects. *Transplantation* **90**, 105–112 (2010).

28. Liu, B., Shyr, Y., Cai, J. & Liu, Q. Interplay between miRNAs and host genes and their role in cancer. *Brief. Funct. Genomics* **18**, 255–266 (2019).

29. Catalanotto, C., Cogoni, C. & Zardo, G. MicroRNA in control of gene expression: An overview of nuclear functions. *Int. J. Mol. Sci.* **17**, (2016).

30. O'Brien, J., Hayder, H., Zayed, Y. & Peng, C. Overview of microRNA biogenesis, mechanisms of actions, and circulation. *Front. Endocrinol. (Lausanne).* **9**, 1–12 (2018).

31. Winter, J., Jung, S., Keller, S., Gregory, R. I. & Diederichs, S. Many roads to maturity: MicroRNA biogenesis pathways and their regulation. *Nat. Cell Biol.* **11**, 228–234 (2009).

32. Shukla, G. C., Singh, J. & Barik, S. MicroRNAs: Processing, maturation, target recognition

and regulatory functions. *Mol. Cell. Pharmacol.* **3**, 83–92 (2011).

33. Yi, R., Qin, Y., Macara, I. G. & Cullen, B. R. Exportin-5 mediates the nuclear export of pre-microRNAs and short hairpin RNAs. *Genes Dev.* **17**, 3011–3016 (2003).

34. Sheu-Gruttadauria, J. & MacRae, I. J. Structural Foundations of RNA Silencing by Argonaute. *J. Mol. Biol.* **429**, 2619–2639 (2017).

35. Mulrane, L., McGee, S. F., Gallagher, W. M. & O'Connor, D. P. miRNA dysregulation in breast cancer. *Cancer Res.* **73**, 6554–6562 (2013).

36. McDermott, A. M., Heneghan, H. M., Miller, N. & Kerin, M. J. The therapeutic potential of microRNAs: Disease modulators and drug targets. *Pharm. Res.* **28**, 3016–3029 (2011).

37. Guo, Z. W. *et al.* MtiBase: A database for decoding microRNA target sites located within CDS and 5′UTR regions from CLIP-Seq and expression profile datasets. *Database* **2015**, 1–9 (2015).

38. Liu, H. *et al.* Nuclear functions of mammalian MicroRNAs in gene regulation, immunity and cancer. *Mol. Cancer* **17**, 1–14 (2018).

39. Oliveto, S., Mancino, M., Manfrini, N. & Biffo, S. Role of microRNAs in translation regulation and cancer. *World J. Biol. Chem.* **8**, 45 (2017).

40. Li, M. *et al.* MicroRNAs: Control and loss of control in human physiology and disease. *World J. Surg.* **33**, 667–684 (2009).

41. Conti, I. *et al.* miRNAs as Influencers of Cell-Cell Communication in Tumor Microenvironment. *Cells* **9**, 1–28 (2020).

42. Iorio, M. V. & Croce, C. M. MicroRNA dysregulation in cancer: Diagnostics, monitoring and therapeutics. A comprehensive review. *EMBO Mol. Med.* **4**, 143–159 (2012).

43. Condrat, C. E. *et al.* miRNAs as Biomarkers in Disease: Latest Findings Regarding Their Role in Diagnosis and Prognosis. *Cells* **9**, 1–32 (2020).

44. Lubov, J. *et al.* Meta-analysis of micrornas expression in head and neck cancer: Uncovering association with outcome and mechanisms. *Oncotarget* **8**, 55511–55524 (2017).

45. Ganci, F. *et al.* Altered peritumoral microRNA expression predicts head and neck cancer patients with a high risk of recurrence. *Mod. Pathol.* **30**, 1387–1401 (2017).

46. Citron, F. *et al.* An integrated approach identifies mediators of local recurrence in head and neck squamous carcinoma. *Clin. Cancer Res.* **23**, 3769–3780 (2017).

47. Citron, F. *et al.* miR-9 modulates and predicts the response to radiotherapy and EGFR inhibition in HNSCC. *EMBO Mol. Med.* 1–20 (2021). doi:10.15252/emmm.202012872

48. White, R. A. *et al.* Epithelial stem cell mutations that promote Squamous cell carcinoma metastasis. *J. Clin. Invest.* **123**, 4390–4404 (2013).

49. Salazar, C. *et al.* A novel saliva-based microRNA biomarker panel to detect head and neck cancers. *Cell. Oncol.* **37**, 331–338 (2014).

50. Black, A. R., Black, J. D. & Azizkhan-Clifford, J. Sp1 and Kruppel-like Transcription Factors in Cell Growth Regulation and Cancer. *J. Cell. Physiol.* **188**, 143–160 (2001).

51. Kim, C. K., He, P., Bialkowska, A. B. & Yang, V. W. SP and KLF Transcription Factors in Digestive Physiology and Diseases. *Gastroenterology* **152**, 1845–1875 (2017).

52. Suske, G., Bruford, E. & Philipsen, S. Mammalian SP/KLF transcription factors: Bring in the family. *Genomics* **85**, 551–556 (2005).

53. McConnell, B. B. & Yang, V. W. *Mammalian Krüppel-Like Factors in Health and Diseases*. *Physiological Reviews* **90**, (2010).

54. Turner, J. & Crossley, M. Mammalian Kruppel-like transcription factors: More than just a pretty finger. *Trends Biochem. Sci.* **24**, 236–240 (1999).

55. Lania, L., Majello, B. & De Luca, P. Transcriptional regulation by the Sp family proteins. *Int. J. Biochem. Cell Biol.* **29**, 1313–1323 (1997).

56. Limame, R., Beeck, K. Op De, Lardon, F. & Wever, O. De. Krüppel-like factors in cancer progression : three fingers on the steering wheel . ABSTRACT : *J. Biol. Chem.* **5**, (2013).

57. Gao, Y., Ding, Y., Chen, H., Chen, H. & Zhou, J. Targeting Kruppel-Like Factor 5 (KLF5) for Cancer Therapy. *Curr. Top. Med. Chem.* **15**, 699–713 (2015).

58. Yang, V. W. Krüppel-like factors in cancers. *Biol. Krüppel-like Factors* **13**, 205–219 (2009).

59. Diakiw, S. M., D'Andrea, R. J. & Brown, A. L. The double life of KLF5: Opposing roles in regulation of gene-expression, cellular function, and transformation. *IUBMB Life* **65**, 999–1011 (2013).

60. Schaeper, N. D., Prpic, N. M. & Wimmer, E. A. A clustered set of three Sp-family genes is ancestral in the Metazoa: Evidence from sequence analysis, protein domain structure, developmental expression patterns and chromosomal location. *BMC Evol. Biol.* **10**, (2010).

61. Beishline, K. & Azizkhan-Clifford, J. Sp1 and the 'hallmarks of cancer'. *FEBS J.* **282**, 224–258 (2015).

62. Vellingiri, B. *et al.* Understanding the role of the transcription factor sp1 in ovarian cancer: From theory to practice. *Int. J. Mol. Sci.* **21**, (2020).

63. Vizcaíno, C., Mansilla, S. & Portugal, J. Sp1 transcription factor: A long-standing target in cancer chemotherapy. *Pharmacol. Ther.* **152**, 111–124 (2015).

64. Bouwman, P. & Philipsen, S. Regulation of the activity of Sp1-related transcription factors. *Mol. Cell. Endocrinol.* **195**, 27–38 (2002).

65. Chu, S. Transcriptional regulation by post-transcriptional modification-Role of phosphorylation in Sp1 transcriptional activity. *Gene* **508**, 1–8 (2012).

66. de Borja, P. F., Collins, N. K., Du, P., Azizkhan-Clifford, J. & Mudryj, M. Cyclin A-CDK phosphorylates Sp1 and enhances Sp1-mediated transcription. *EMBO J.* **20**, 5737–5747 (2001).

67. Yang, H. C. *et al.* Pin1-mediated Sp1 phosphorylation by CDK1 increases Sp1 stability and decreases its DNA-binding activity during mitosis. *Nucleic Acids Res.* **42**, 13573–13587 (2014).

68. Olofsson, B. A., Kelly, C. M., Kim, J., Hornsby, S. M. & Azizkhan-Clifford, J. Phosphorylation of Sp1 in response to DNA damage by ataxia telangiectasia-mutated kinase. *Mol. Cancer Res.* **5**, 1319–1330 (2007).

69. Lee, J. A. *et al.* Transcriptional activity of Sp1 is regulated by molecular interactions between the zinc finger DNA binding domain and the inhibitory domain with corepressors, and this interaction is modulated by MEK. *J. Biol. Chem.* **280**, 28061–28071 (2005).

70. O'Connor, L., Gilmour, J. & Bonifer, C. The role of the ubiquitously expressed transcription factor Sp1 in tissue-specific transcriptional regulation and in disease. *Yale J. Biol. Med.* **89**, 513–525 (2016).

71. Pollak, N. M., Hoffman, M., Goldberg, I. J. & Drosatos, K. Krüppel-Like Factors: Crippling and Uncrippling Metabolic Pathways. *JACC Basic to Transl. Sci.* **3**, 132–156 (2018).

72. Schuierer, M. *et al.* Induction of AP-2α Expression by Adenoviral Infection Involves Inactivation of the AP-2rep Transcriptional Corepressor CtBP1. *J. Biol. Chem.* **276**, 27944–27949 (2001).

73. Evans, P. M. *et al.* Krüppel-like factor 4 is acetylated by p300 and regulates gene transcription via modulation of histone acetylation. *J. Biol. Chem.* **282**, 33994–34002 (2007).

74. Lomberk, G. & Urrutia, R. The family feud: Turning off Sp1 by Sp1-like KLF proteins. *Biochem. J.* **392**, 1–11 (2005).

75. Swamynathan, S. K. Krüppel-like factors: Three fingers in control. *Hum. Genomics* **4**, 263–270 (2010).

76. Zhang, J., Li, G., Feng, L., Lu, H. & Wang, X. Krüppel-like factors in breast cancer: Function, regulation and clinical relevance. *Biomed. Pharmacother.* **123**, 109778 (2020).

77. Bell, K. N. & Shroyer, N. F. Krüpple-Like Factor 5 Is Required for Proper Maintenance of Adult Intestinal Crypt Cellular Proliferation. *Dig. Dis. Sci.* **60**, 86–100 (2015).

78. Dong, J. T. & Chen, C. Essential role of KLF5 transcription factor in cell proliferation and differentiation and its implications for human diseases. *Cell. Mol. Life Sci.* **66**, 2691–2706 (2009).

79. Farrugia, M. K., Vanderbilt, D. B., Salkeni, M. A. & Ruppert, J. M. Kruppel-like pluripotency factors as modulators of cancer cell therapeutic responses. *Cancer Res.* **76**, 1677–1682 (2016).

80. Ma, D. *et al.* KLF5 promotes cervical cancer proliferation, migration and invasion in a manner partly dependent on TNFRSF11a expression. *Sci. Rep.* **7**, 1–13 (2017).

81. Chen, C. *et al.* Ubiquitin-proteasome degradation of KLF5 transcription factor in cancer and untransformed epithelial cells. *Oncogene* **24**, 3319–3327 (2005).

82. Guo, P., Xing, C., Fu, X., He, D. & Dong, J. T. Ras inhibits TGF-β-induced KLF5

acetylation and transcriptional complex assembly via regulating SMAD2/3 phosphorylation in epithelial cells. *J. Cell. Biochem.* **121**, 2197–2208 (2020).

83. Dong, Z., Yang, L. & Lai, D. KLF5 strengthens drug resistance of ovarian cancer stem-like cells by regulating survivin expression. *Cell Prolif.* **46**, 425–435 (2013).

84. Lee, S. J. *et al.* Regulation of hypoxia-inducible factor 1α (HIF-1α) by lysophosphatidic acid is dependent on interplay between p53 and Krüppel-like factor 5. *J. Biol. Chem.* **288**, 25244–25253 (2013).

85. Li, M. *et al.* Krüppel-like factor 5 promotes epithelial proliferation and DNA damage repair in the intestine of irradiated mice. *Int. J. Biol. Sci.* **11**, 1458–1468 (2015).

86. Luo, Y. & Chen, C. The roles and regulation of the KLF5 transcription factor in cancers. *Cancer Sci.* **112**, 2097–2117 (2021).

87. Liu, R. *et al.* Mifepristone suppresses basal triple-negative breast cancer stem cells by down-regulating KLF5 expression. *Theranostics* **6**, 533–544 (2016).

88. Farrugia, M. K. *et al.* Regulation of anti-apoptotic signaling by Kruppel-like factors 4 and 5 mediates lapatinib resistance in breast cancer. *Cell Death Dis.* **6**, e1699 (2015).

89. Bateman, N. W., Tan, D., Pestell, R. G., Black, J. D. & Black, A. R. Intestinal Tumor Progression Is Associated with Altered Function of KLF5. *J. Biol. Chem.* **279**, 12093–12101 (2004).

90. Guo, P. *et al.* Pro-proliferative factor KLF5 becomes anti-proliferative in epithelial homeostasis upon signaling-mediated modification. *J. Biol. Chem.* **284**, 6071–6078 (2009).

91. Du, J. X., Bialkowska, A. B., McConnell, B. B. & Yang, V. W. SUMOylation regulates nuclear localization of Krüppel-like factor 5. *J. Biol. Chem.* **283**, 31991–32002 (2008).

92. Li, X. *et al.* Interruption of KLF5 acetylation converts its function from tumor suppressor to tumor promoter in prostate cancer cells. *Int. J. Cancer* **136**, 536–546 (2015).

93. Li, J. *et al.* Roles of Krüppel-like factor 5 in kidney disease. *J. Cell. Mol. Med.* **25**, 2342–2355 (2021).

94. Yang, Y., Tarapore, R. S., Jarmel, M. H., Tetreault, M. P. & Katz, J. P. P53 mutation alters the effect of the esophageal tumor suppressor KLF5 on keratinocyte proliferation. *Cell Cycle* **11**, 4033–4039 (2012).

95. Li, J.-C. *et al.* The Partial Role of KLF4 and KLF5 in Gastrointestinal Tumors. *Gastroenterol. Res. Pract.* **2021**, 1–13 (2021).

96. Yang, Y. *et al.* Loss of transcription factor KLF5 in the context of p53 ablation drives invasive progression of human squamous cell cancer. *Cancer Res.* **71**, 6475–6484 (2011).

97. Levine, A. J. P53: 800 Million Years of Evolution and 40 Years of Discovery. *Nat. Rev. Cancer* **20**, 471–480 (2020).

98. Aubrey, B. J., Kelly, G. L., Janic, A., Herold, M. J. & Strasser, A. How does p53 induce apoptosis and how does this relate to p53-mediated tumour suppression? *Cell Death Differ.*

25, 104–113 (2018).

99. Stengel, A. *et al.* The impact of TP53 mutations and TP53 deletions on survival varies between AML, ALL, MDS and CLL: An analysis of 3307 cases. *Leukemia* **31**, 705–711 (2017).

100. Klinakis, A. & Rampias, T. TP53 mutational landscape of metastatic head and neck cancer reveals patterns of mutation selection. *EBioMedicine* **58**, (2020).

101. Liebl, M. C. & Hofmann, T. G. The Role of p53 Signaling in Colorectal Cancer. *Cancers (Basel).* **13**, 2125 (2021).

102. Saleh, A. & Perets, R. Mutated p53 in hgsc—from a common mutation to a target for therapy. *Cancers (Basel).* **13**, 1–21 (2021).

103. Frebourg, T. *et al.* Guidelines for the Li–Fraumeni and heritable TP53-related cancer syndromes. *Eur. J. Hum. Genet.* **28**, 1379–1386 (2020).

104. Timmerman, D. M., Remmers, T. L., Hillenius, S. & Looijenga, L. H. J. Mechanisms of tp53 pathway inactivation in embryonic and somatic cells—relevance for understanding (Germ cell) tumorigenesis. *Int. J. Mol. Sci.* **22**, (2021).

105. Brosh, R. & Rotter, V. When mutants gain new powers: News from the mutant p53 field. *Nat. Rev. Cancer* **9**, 701–713 (2009).

106. Kim, M. P. & Lozano, G. Mutant p53 partners in crime. *Cell Death Differ.* **25**, 161–168 (2018).

107. Freed-Pastor, W. A. & Prives, C. Mutant p53: One name, many proteins. *Genes Dev.* **26**, 1268–1286 (2012).

108. Pfister, N. T. & Prives, C. and Cancer-Related Mutant Forms of p53. 1–26 (2017).

109. Kastenhuber, E. R. & Lowe, S. W. Putting p53 in Context. *Cell* **170**, 1062–1078 (2017).

110. Zhang, C. *et al.* Gain-of-function mutant p53 in cancer progression and therapy. *J. Mol. Cell Biol.* **12**, 674–687 (2020).

111. Zhou, G., Liu, Z. & Myers, J. N. TP53 Mutations in Head and Neck Squamous Cell Carcinoma and Their Impact on Disease Progression and Treatment Response. *J. Cell. Biochem.* **2692**, 2682–2692 (2016).

112. Caponio, V. C. A. *et al.* Computational analysis of TP53 mutational landscape unveils key prognostic signatures and distinct pathobiological pathways in head and neck squamous cell cancer. *Br. J. Cancer* **123**, 1302–1314 (2020).

113. Kaczynski, J., Cook, T. & Urrutia, R. Protein family review Sp1- and Krüppel-like transcription factors. *Genome Biol.* 1–8 (2003).

114. Kim, E. & Deppert, W. Transcriptional activities of mutant p53: When mutations are more than a loss. *J. Cell. Biochem.* **93**, 878–886 (2004).

115. Koutsodontis, G., Vasilaki, E., Chou, W. C., Papakosta, P. & Kardassis, D. Physical and

functional interactions between members of the tumour suppressor p53 and the Sp families of transcription factors: Importance for the regulation of genes involved in cell-cycle arrest and apoptosis. *Biochem. J.* **389**, 443–455 (2005).

116. Pavlakis, E. & Stiewe, T. p53's extended reach: The mutant p53 secretome. *Biomolecules* **10**, (2020).

117. Weisz, L., Oren, M. & Rotter, V. Transcription regulation by mutant p53. *Oncogene* **26**, 2202–2211 (2007).

118. Ghaleb, A. M. & Yang, V. W. Krüppel-like factor 4 (KLF4): What we currently know. *Gene* **611**, 27–37 (2017).

119. Cordani, N. *et al.* Mutant p53 subverts p63 control over KLF4 expression in keratinocytes. *Oncogene* **30**, 922–932 (2011).

120. Rowland, B. D., Bernards, R. & Peeper, D. S. The KLF4 tumour suppressor is a transcriptional repressor of p53 that acts as a context-dependent oncogene. *Nat. Cell Biol.* **7**, 1074–1082 (2005).

121. Zhu, N. *et al.* KLF5 interacts with p53 in regulating survivin expression in acute lymphoblastic leukemia. *J. Biol. Chem.* **281**, 14711–14718 (2006).

122. Xia, W., Bai, H., Deng, Y. & Yang, Y. PLA2G16 is a mutant p53/KLF5 transcriptional target and promotes glycolysis of pancreatic cancer. *J. Cell. Mol. Med.* **24**, 12642–12655 (2020).

123. Sun, L. *et al.* KLF5 regulates epithelial-mesenchymal transition of liver cancer cells in the context of p53 loss through miR-192 targeting of ZEB2. *Cell Adhes. Migr.* **14**, 182–194 (2020).

124. Nicolás, M., Noé, V., Jensen, K. B. & Ciudad, C. J. Cloning and Characterization of the 5′-Flanking Region of the Human Transcription Factor Sp1 Gene. *J. Biol. Chem.* **276**, 22126–22132 (2001).

125. Ma, L. *et al.* MiR-9, a MYC/MYCN-activated microRNA, regulates E-cadherin and cancer metastasis. *Nat. Cell Biol.* **12**, 247–256 (2010).

126. Zhang, J. P. *et al.* Down-regulation of Sp1 suppresses cell proliferation, clonogenicity and the expressions of stem cell markers in nasopharyngeal carcinoma. *J. Transl. Med.* **12**, 1–12 (2014).

127. Fletcher, S. C. *et al.* Sp1 phosphorylation by ATM downregulates BER and promotes cell elimination in response to persistent DNA damage. *Nucleic Acids Res.* **46**, 1834–1846 (2018).

128. Xing, C. *et al.* Klf5 deletion promotes pten deletion-initiated luminal-type mouse prostate tumors through multiple oncogenic signaling pathways. *Neoplasia (United States)* **16**, 883–899 (2014).

129. Yang, D. *et al.* The long non-coding RNA TUG1-miR-9a-5p axis contributes to ischemic injuries by promoting cardiomyocyte apoptosis via targeting KLF5. *Cell Death Dis.* **10**, (2019).

130. Healy, S., Khan, P. & Davie, J. R. Immediate early response genes and cell transformation. *Pharmacol. Ther.* **137**, 64–77 (2013).

AKNOWLEDGEMENTS

This work was performed in the division of Molecular Oncology at National Cancer Institute (CRO) of Aviano, directed by Dr. Gustavo Baldassarre.

First, I would like to thank dears Dr. Barbara Belletti and Dr. Gustavo Baldassarre for having me given the great opportunity to carry out the PhD research in a working context like CRO. Working with them on this project allowed me to meet beautiful personalities and to compare myself with as many esteemed scientists and this was an immense honor for me. Thanks for all the advice that I will treasure, for the scientific support and the trust, for all the time dedicated to me in full authenticity and professionalism.

I'm really grateful to all the other members of SCICC group. Each one of you made my PhD a stimulating and joyful experience placed inside and outside the laboratory, supporting and teaching me a lot! In your own way, you contributed to my research project by enriching its contents.

I wish to thank dear Dr. Michele Avanzo of Radiotherapy Unit in CRO for his technical support and Dr. Francesca Citron for her scientific contribution.

Thanks so much to all the CRO members, a small family that never stops fighting against cancer.